Development of a genetically encoded chemiluminescent voltage indicator and its application to biological research

Shigenori Inagaki,

Osaka University

A thesis submitted to Graduate School of Frontier Biosciences for the Degree of Doctor of Philosophy

March, 2018

General introduction

Membrane voltage stems from the difference in electric potential across the outside and inside of the plasma membrane. Excitable cells, such as neurons and cardiomyocytes, utilize the change in membrane voltage as an electrical signal, and propagate it to neighboring cells. In our brain, more than one hundred billion neurons communicate with each other via synaptic connections forming complicated neural circuits, that allow high order brain functions such as memory and emotion. Also, our heart beats with regularity and precision according to periodic propagation of electrical signals among cardiomocytes. Therefore, to understand the basis of the cooperative activity, we have to know the actual dynamics of membrane voltage among the cells.

The techniques to measure membrane voltage have been developed based on electrophysiology and fluorescent imaging. Among them, Genetically Encoded Voltage Indicators (GEVIs) are attracting attention in the field of neuroscience and cardiology. Since the expression of these indicators can be regulated under the cell-specific promoter, one can measure the membrane voltage from genetically defined cell subpopulations, which is quite challenging with other techniques. However, to obtain the fluorescent signal reflecting membrane voltage, excitation light has to be irradiated to the specimen. In such a case, damage to the samples (phototoxicity), high-background noise from autofluorescence and rapid reduction in fluorescence intensity due to photobleaching cannot be avoided. Also, when the experiment needs to be combined with optotogenetic stimulation using e.g. channelrhodopsin2 (ChR2), the excitation light for GEVIs easily activates highly light-sensitive optogenetic actuators. More importantly, to perform brain activity imaging, an animal must be head-fixed or connected to an optical fiber, limiting the investigation of neural networks during social behavior such as caregiving, mating and fighting

To solve these problems derived from excitation light, I focused on bioluminescence (chemiluminescence) imaging. A chemiluminescent protein is an enzyme that catalyzes the oxidative reaction of a substrate, driving light generation

without an external light source. Through the rational design and screening, finally I developed the world's first chemiluminescent voltage indicator, LOTUS-V consisting of a cyan-emitting chemiluminescent protein (NLuc), a yellow fluorescent protein (Venus) and a voltage-sensing domain. While membrane voltage is depolarized, the structure change of LOTUS-V shortens the distance between NLuc and Venus, enhancing energy transfer from NLuc to Venus. Thus, one can measure membrane voltage based on the color shift of luminescence from LOTUS-V. *In vitro* experiments with LOTUS-V enabled robust and sensitive drug evaluation, and long-term recording in cardiomyocytes derived from human-induced pluripotent stem cells without phototoxicity and autofluorescence. Also, it successfully visualized both depolarization and hyperpolarization of membrane voltage caused by simultaneous use of multiple optogenetic actuators. For *in vivo* experiments, I developed a novel fiber-free imaging system in conjunction with LOTUS-V, allowing brain activity recording in several unrestrained animals simultaneously for 7 h at most. With this system, I identified a novel type of activation in the primary visual cortex, associated with the freely moving state and interaction with other mice.

Collectively, LOTUS-V offers the multiple advantages of chemiluminescence imaging, and thus expands the toolbox for voltage recording in cells and intact animals. It would be prevailed for drug screening in cardiomyocytes or animals, and for investigation of an unexplored activity in various brain regions relating to animal's social or group behavior.

Abstract

Bioluminescence (chemiluminescence) imaging is attracting attention in the field of biology due to its superior signal-to-background ratio and capacity for long-tem measurement. Also, since it does not require excitation light unlike fluorescence imaging, unrestricted optogenetic manipulation using e.g. channelrhodopsin2 can be easily integrated with imaging. In this thesis, I report the world's first chemiluminescent voltage indicator, LOTUS-V enabling investigation of voltage dynamics without the limitations that are often problematic in current techniques. *In vitro* experiments with LOTUS-V enabled robust and sensitive drug evaluation, and long-term recording in cardiomyocytes derived from human-induced pluripotent stem cells. Also, it successfully visualized the bidirectional changes in membrane voltage caused by simultaneous use of multiple optogenetic actuators. For *in vivo* experiments, I developed a novel fiber-free imaging system in conjunction with LOTUS-V, allowing detection of electrophysiological field potential dynamics in the brains of several unrestrained animals simultaneously. With this system, I identified a novel type of activation in the primary visual cortex, associated with the freely moving state and interaction with other mice, suggesting that it may investigate an unexplored activity in various brain regions relating to social or group behavior. Collectively, LOTUS-V offers the multiple advantages of chemiluminescence imaging, and thus expands the toolbox for voltage recording in cells and intact animals.

Index

CHAPTER 3

IN VITRO DRUG EVALUATION

CHAPTER 4

IN VITRO OPTOGENETIC STIMULATION

2. Abbreviations

- **AAV**: adeno-associated virus
- **Abs.**: absorption
- **ADC** count: analogue-to-digital converter count
- **APD**: action potential duration
- **AST**: astemizole
- **ArchT**: archaerhodopsinT
- **Ca^{2+}**: calcium ion
- **ChR2**: channelrhodopsin 2
- **Ci-VSP**: voltage-sensing phosphatase from *Ciona intestinalis*
- **cp**: circular permuted
- **Dead time**: duration of the processes for image readout and accumulated charge clearing on the camera
- **DIC**: differential interference contrast
- **DIV**: day *in vitro*
- **DMEM**: Dulbecco's modified Eagle's medium
- **EEG**: electroencephalography
- **eNpHR**: halorhodopsin
- **FBS**: fetal bovine serum
- **FP**: fluorescent protein
- **FRET**: Förster resonance energy transfer
- **GEVI**: genetically encoded voltage indicator
- **Gg-VSD**: voltage sensing domain from Gg-VSP
- **Gg-VSP**: voltage-sensing phosphatase from *Gallus gallus*
- **GH3 cell**: rat pituitary epithelial-like tumor cell
- **H^+**: proton
- **HBSS**: Hanks' balanced salt solution
- **HEK293T cell**: human embryonic kidney 293T cell
- **hERG channel**: human ether-a-go-go related channel
- **HS**: horse serum
- **hESC**: human-embryonic stem cell
- **hiPSC**: human-induced pluripotent stem cell

- **hiPSC-CM**: cardiomyocyte derived from human induced pluripotent stem cells
- **IFU**: infectious units
- **ISO**: isoproterenol
- **KCl**: potassium chloride
- **LED**: light emitting diode
- **LFP**: local field potential
- **LOTUS-V**: luminescent optical tool for universal sensing of voltage
- **NADPH**: nicotinamide adenine dinucleotide phosphate
- **NGF**: nerve growth factor
- **PC12 cells**: pheochromocytoma cells
- **PCR**: polymerase chain reaction
- **PTEN**: phosphatase and tensin homolog
- **QT interval**: duration between the start of Q wave and the end of T wave
- **ROI**: region of interest
- **SBR**: signal-to-background ratio
- **TIRF microscope**: total internal reflection fluorescence microscope
- **TTL**: transistor-transistor logic
- **TTX**: tetrodotoxin
- **V1**: primary visual cortex
- **$V_{1/2}$:** half-maximal activation against applied voltages
- **VSD**: voltage-sensing domain

Chapter1 ENGINEERING A CHEMILUMINESCENT VOLTAGE INDICATOR

1.1. Introduction

1.1.1. Physiological significance of membrane voltage

Membrane voltage stems from the difference in electric potential across the outside and inside of the plasma membrane. Excitable cells, such as neurons, utilize the change in membrane voltage as an electrical signal, and propagate it to neighboring cells. In our brain, more than one hundred billion neurons communicate with each other via synaptic connections forming complicated neural circuits, that allow high order brain functions such as memory and emotion. Therefore, a worthy mission for neuroscientists is to reveal how electrical signals are cooperatively, and harmonically, integrated to generate high-order brain activity.

1.1.2. Genetically encoded voltage indicators (GEVIs)

Genetically encoded voltage indicators (GEVIs) are gaining prominence in neuroscience and cardiovascular research (1). The advantage of GEVIs is that they allow voltage recording from genetically defined cell populations, which is otherwise challenging with other techniques based on electrophysiology or optics. Conventional GEVIs have been designed for fluorescence imaging to date and classified mainly into two types depending on the voltage-sensing domain. One type are the VSD-based GEVIs (2–4), which use a voltage-sensing domain (VSD) of either voltage-sensing phosphatase from *Ciona intestinalis* (Ci-VSP) (5) or *Gallus gallus* (Gg-VSP) (**Fig.1a-b**)

(4). Ci-VSP and Gg-VSP are composed of a four-pass transmembrane protein, and a phosphatase and a tensin homolog (PTEN) like protein, which dephosphorylates inositol phospholipid when membrane voltage is depolarized. VSDs contain several positively charged amino acids such as arginine and lysine mainly in the S4 domain, and thus change structure depending on membrane voltage. Various kinds of GEVIs utilize these structural dynamics to enhance/reduce Förster resonance energy transfer (FRET) efficiency between donor and acceptor fluorescent proteins (**Fig.1a**) (2, 6, 7) or change the microenvironment surrounding the chromophore of a fluorescent protein (**Fig.1b**) (3, 4, 8). The second type are rhodopsin-based GEVIs (**Fig.1c-d**) (9, 10), which use archaerhodopsin as the voltage-sensing domain. Archaerhodopsin (for instance, Archaerhodopsin 3) is originally a light-driven H^+ pump and used as an optogenetic actuator. It can be used to suppress neural activity by pumping out intracellular H^+ to the extracellular space (9, 11). Archaerhodopsin has all-trans-retinal as a chromophore, conjugated to a lysine residue through a Schiff-base linkage. Although the quantum yield of fluorescence emission is quite low ($0.4\text{-}5\times10^{-3}$), the archaerhodopsin, designed not to pump out intracellular H^+, senses the depolarization/hyperpolarization of membrane voltage and changes fluorescence intensity (**Fig.1c**) (9, 10). It is considered that protonation/deprotonation of the Schiff base plays a key roll in its voltage sensitivity. More recently, an indicator composed of archaerhodopsin and a fluorescent protein has been reported (**Fig.1d**) (12–14). The emission intensity from the fluorescent protein moiety decreases upon depolarization of membrane voltage due to the increase of FRET efficiency, thus overcoming the problem

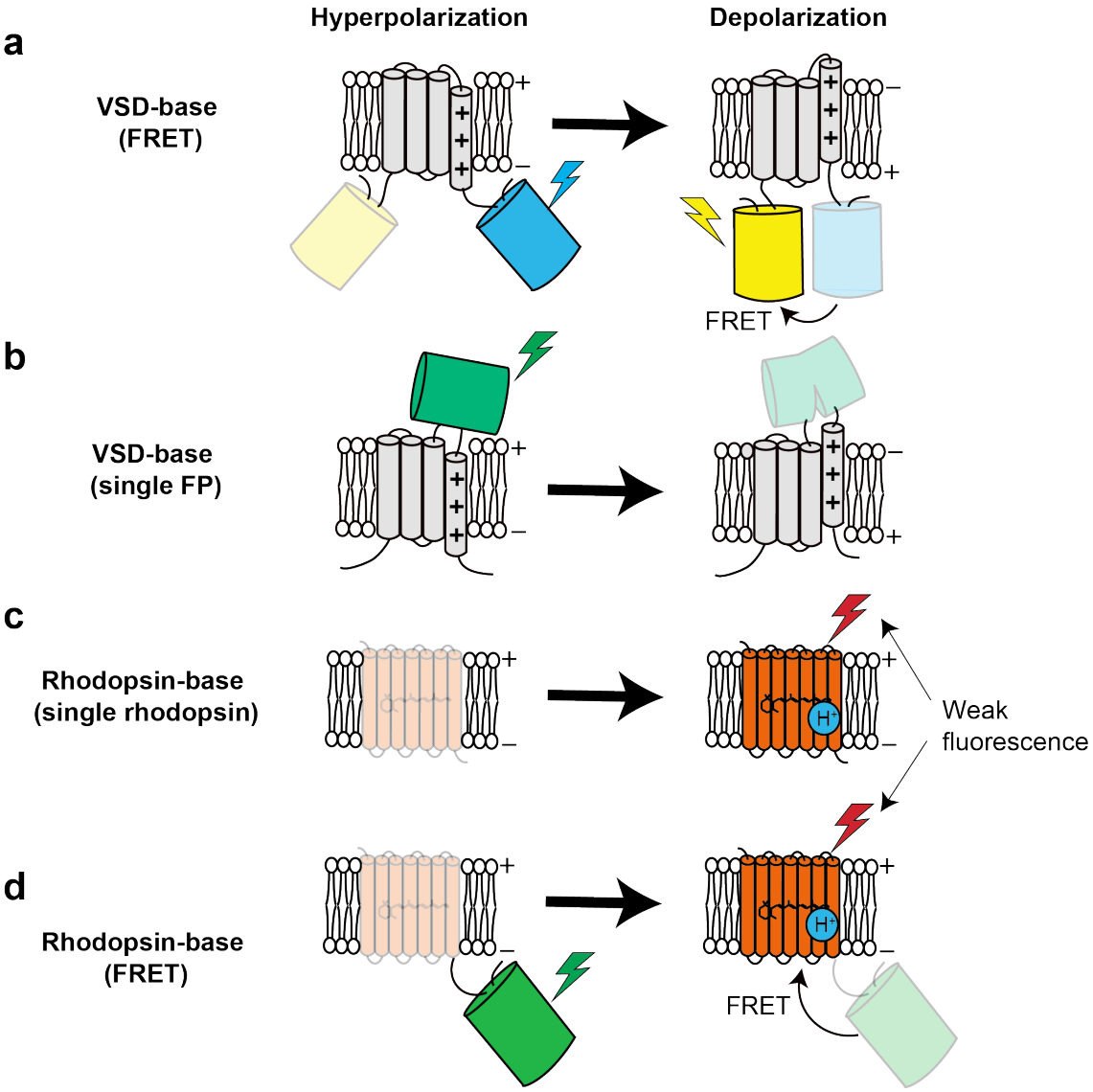

Figure 1 Schematic diagrams of (a-b) VSD and (c-d) rhodopsin-based GEVIs. (**a**) VSD-based voltage indicator utilizing FRET between a donor (blue) and acceptor (yellow) fluorescent proteins (FPs). (**b**) VSD-based voltage indicator utilizing a circularly permuted (cp) GFP (green). (**c**) Rhodopsin-based voltage indicator changes its fluorescence emission by protonation/deprotonation of the Schiff base, caused by a voltage change. (**d**) Rhodopsin-based voltage indicator utilizing FRET to quench a donor FP (green).

of low fluorescence intensity.

Both types of indicators are widely used but have several distinct features.

VSD-based indicators have higher expression level, better localization to the plasma membrane and adequate voltage sensitivity in two-photon imaging, however the dynamic range and voltage response kinetics are not as good as rhodopsin-based GEVIs (1). Unfortunately, rhodopsin-based indicators are incompatible with two-photon excitation probably because of complicated photocycles of all-trans retinal (15).

1.1.3. Limitations of current voltage imaging

Usually, the power density of excitation light for voltage imaging is around ~1 W/cm^2, or ~2000 W/cm^2 for Archaerhodopsin 3-type indicators (9, 10, 14, 16, 17). At such high-power density, damage to the samples (phototoxicity), high-background noise from autofluorescence and rapid reduction in fluorescence intensity due to photobleaching cannot be avoided (17). Also, when the experiment needs to be combined with optotogenetic stimulation using e.g. channelrhodopsin2 (ChR2) (18), the excitation light for GEVIs easily activates highly light-sensitive optogenetic actuators (17). More importantly, to perform brain activity imaging, an animal must be head-fixed or connected to an optical fiber, limiting the investigation of neural networks during complicated behavior such as caregiving, mating and fighting (6, 7, 14, 19).

1.2. Purpose and significance

The best way to overcome such limitations is to perform chemiluminescence imaging. A chemiluminescent protein is an enzyme that catalyzes the oxidative reaction of a substrate, driving light generation without an external light source (20). Thus, I decided

to develop a chemiluminescent voltage indicator to avoid forementioned problems and expand the applicability of voltage imaging to complex biology.

1.3. Materials and methods

Gene construction. The DNA fragments for the C-terminal portion of VSD(R217Q) were amplified by KOD polymerase chain reaction (PCR) from pCS4+-Mermaid2, using a sense primer containing an *Eco*RI site and a reverse primer containing an *Xho*I site. The DNA fragments of mNeonGreen (a greenish yellow fluorescent protein, Allele Biotechnology) (21), Venus (a yellow fluorescent protein) (22), or circularly permuted (cp)Venus (23) by KOD PCR using a sense primer containing an *Xho*I site and a reverse primer containing a *Not*I site and a stop codon. These fragments were ligated with pcDNA3 (Invitrogen) digested by *Eco*RI and *Not*I to make pcDNA3-VSD_C-FP. The DNA fragments for the N-terminal portion of VSD(R217Q) were amplified by KOD PCR using a sense primer containing a Kozak sequence following a *Hin*dIII site and a reverse primer containing a *Bam*HI site. The DNA fragment for NanoLuc (Promega) (24) was amplified by KOD PCR using a sense primer containing a *Bam*HI site and a reverse primer containing an *Eco*RI site. These fragments were ligated with pcDNA3-VSD_C-FP digested by *Hin*dIII and *Bam*HI to finally make pcDNA3-N_VSD-NLuc-VSD_C-FP. Constructs where a fluorescent protein and NanoLuc were located at the N and C-terminus portion of VSD(R217Q) respectively were created with the same procedure. The Y66G and D129R mutations inside Venus and the VSD(R217Q) respectively were introduced by PCR mutagenesis using a sense

primer (25). All constructs were verified by DNA sequencing, primers are listed in **Table1**.

Screening by KCl stimulation. Rat pituitary epithelial-like tumor (GH3) cells (ATCC, CCL-82.1) were cultured in Dulbecco's Modified Eagle's Medium (DMEM): Nutrient Mixture F-12 Ham (DMEM/F12) (Invitrogen) containing 15% horse serum (HS) and 2.5% fetal bovine serum (FBS) at 37°C in air with 5% CO_2. Two days before the screening experiment, the GH3 cells were trypsinized and transferred to homemade 35-mm glass-bottom dishes with glass-surface coated with 0.1 mg/ml poly-D-lysine (Sigma). The next day, candidate constructs were transfected into the cells by Lipofectamine2000 (Invitrogen), following the manufacturer's protocol. Just before the experiment, culture medium was replaced with phenol red-free DMEM/F12 (Invitrogen) and 5 mM stock solution of furimazine (Nano-Glo assay kit, Promega) was applied into the imaging medium up to 50 μM.

The images of donor and acceptor channels were acquired simultaneously using W-VIEW GEMINI image splitting optics (Hamamatsu Photonics) and an iXon Ultra EMCCD camera (Andor Technology). The image splitting optics has a FF509-FDi01-25×36 dichroic mirror (Semrock), FF01-483/32-25 and FF01-525/45-25 emission filters (Semrock). Half way through the imaging protocol, 20 μl of 150 mM potassium chloride (KCl) solution was directly applied to the imaging region to evoke KCl-induced depolarization.

Spectral measurement. Construct-expressing GH3 cells were detached from the dish by a scraper, and suspended in DMEM (Invitrogen) without serum. The suspension was transferred to 96-well plates at a density of 1.2×10^5 cells/well. 5 mM stock solution of furimazine was applied into the suspension up to 5 μM just before the measurement. The chemiluminescence spectrum was measured by a SH-9000 microplate reader (Colona Electric).

Investigation of furimazine toxicity. One day before the experiment, human embryonic kidney 293T (HEK293T) cells (RIKEN BRC Cell Bank, RCB2202) were mounted on collagen-coated 35-mm glass-bottom dishes in DMEM supplemented with 10% FBS. Just before imaging, medium was replaced with phenol red-free DMEM/F12 supplemented with 10% FBS and 1 μM SYTOX AADvanced dead cell stain (Molecular Probes). Cells were continuously irradiated by excitation light for 5 min on an Eclipse Ti-E inverted microscope (Nikon) equipped with a 10x, NA 0.5, Plan Fluor objective lens (Nikon), a FF01-472/30-25 excitation filter and a FF502-Di01 dichroic mirror (Semrock). Cells were maintained at 37°C using a stage-top incubator (Tokai Hit). The illumination power was measured above the objective using a power meter (Thorlabs). Irradiated cells were subsequently observed using Differential Interference Contrast (DIC) and fluorescence images of SYTOX for the following 12 h at 10 min interval. The fluorescence of SYTOX was measured with a FF01-472/30-35 excitation filter, a FF502-Di01 dichroic mirror and a FF01-641/75 emission filter (Semrock). For treatment with furimazine, the medium was replaced with phenol red-free DMEM/F12

supplemented with 10% FBS, 1 μM SYTOX AADvanced dead cell stain and 50 μM furimazine. Then the cells were observed in an identical microscope setup for the following 12 h at 10 min interval.

Data Analysis. Data was analyzed by ImageJ and R software. The activity of GH3 cells was measured by calculating the FRET ratio (R) of an indicator (acceptor signal divided by donor signal). Before calculation of the FRET ratio, the background signal measured in a region of interest (ROI) randomly chosen and placed in a non-specimen area was subtracted from the signal of the specimen in each channel. The change in the FRET ratio ($\Delta R/R_0$) was calculated by subtracting the average value of baseline (R_0) from individual raw values at each time point ($\Delta R = R\text{t} - R_0$; Rt is a raw ratio value at time point "t") and dividing the ΔR by R_0. "Baseline" means that the cells were at the resting membrane potential. Each single image taken through the image splitting optics contains the information of donor and acceptor channels on either the left or right side of the image. The specimen ROI was created from a mask image, made based on an averaged picture over all frames of each movie and a threshold for the chemiluminescence intensity manually decided to cover the expressing area.

1.4. Results and discussion

1.4.1. Design and screening of chemiluminescence voltage indicators

The dynamics of membrane voltage are much faster than Ca^{2+} dynamics, and thus a bright chemiluminescent protein was needed for fast acquisition to generate enough

photons in each image. Therefore, I chose NanoLuc that had been the brightest chemiluminescent proteins at the time (24). Since chemiluminescence intensity highly relies on substrate concentration, which is not totally constant throughout the measurement, I attempted to make a FRET-based indicator using NanoLuc (a FRET donor), a fluorescent protein (a FRET acceptor) and a VSD from Ci-VSP. The structural change upon depolarization was expected to enhance FRET efficiency between NanoLuc and a fluorescent protein, and causes higher intensity ratio (acceptor/donor intensities). This ratiometry could mitigate artifacts such as baseline drift caused by substrate consumption and motion artifact. To develop such a chemiluminescent voltage

N-VSD(1-**X**)	**A**	C-VSD((**X**+1)-**Y**)	**B**

Name	X	Y	A	B
69NL-VSD-249mNG	69	249	NanoLuc	mNeon
69NL-VSD-249VN	69	249	NanoLuc	Venus
84NL-VSD-249mNG	84	249	NanoLuc	mNeon
84NL-VSD-249VN	84	249	NanoLuc	Venus
103NL-VSD-249mNG	103	249	NanoLuc	mNeon
103NL-VSD-249VN (LOTUS-V)	103	249	NanoLuc	Venus
103NL-VSD(D129R)-VN (LOTUS-V(D129R))	103	249	NanoLuc	Venus
103NL-VSD-249VN(cp50)	103	249	NanoLuc	cp50Venus
103NL-VSD-249VN(cp157)	103	249	NanoLuc	cp157Venus
103NL-VSD-249VN(cp173)	103	249	NanoLuc	cp173Venus
103NL-VSD-249VN(cp195)	103	249	NanoLuc	cp195Venus
103NL-VSD-249VN(cp229)	103	249	NanoLuc	cp229Venus
103NL-VSD-243VN	103	243	NanoLuc	Venus
103NL-VSD-239VN	103	239	NanoLuc	Venus
103VN-VSD-249NL	103	249	Venus	NanoLuc
103VN-VSD-243NL	103	243	Venus	NanoLuc
103VN-VSD-239NL	103	239	Venus	NanoLuc

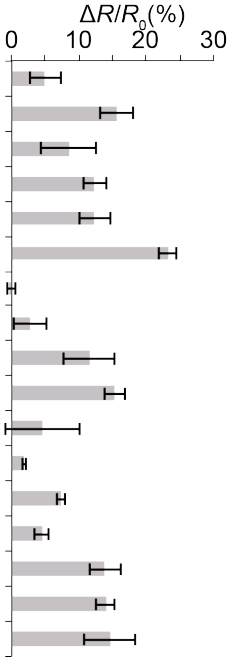

Figure 2 Characterization of chemiluminescnt voltage indicators with KCl stimulation. Multiple combinations of insertion (X), linker sites (Y), FRET donors and acceptors (A or B) were tested. $\Delta R/R_0$ in each construct to KCl-induced depolarization is shown in the right panel. Error bars indicate mean ± SE. The figure is from reference (17).

indicator, various combinations and alignments of NanoLuc and a FRET acceptor were tested (**Fig.2**). These constructs were successfully expressed in GH3 cells and KCl-induced depolarization was evoked to identify the construct with the biggest signal change.

The construct in which NanoLuc was placed between amino acid residues 103 and 104 of VSD(R217Q), whose Venus was conjugated at the C-terminus of VSD(R217Q) showed the highest ratio change ($\Delta R/R_0$) with small deviation ($\Delta R/R_0$=22.6±0.9% [mean ± SE], n=5 cells) (**Fig.2**). I designated it as LOTUS-V (Luminescent Optical Tool for Universal Sensing of Voltage) (**Fig.3**). The D129R mutant of the VSD(R217Q) was previously shown to be insensitive to voltage changes in the physiological range (26). I found that a corresponding mutation in VSD(R217Q) moiety of LOTUS-V abolished the FRET change upon KCl stimulation in GH3 cells ($\Delta R/R_0$=−2.3±2.4% [mean ± SE], n=5 cells, p=0.0090 against the signal change of

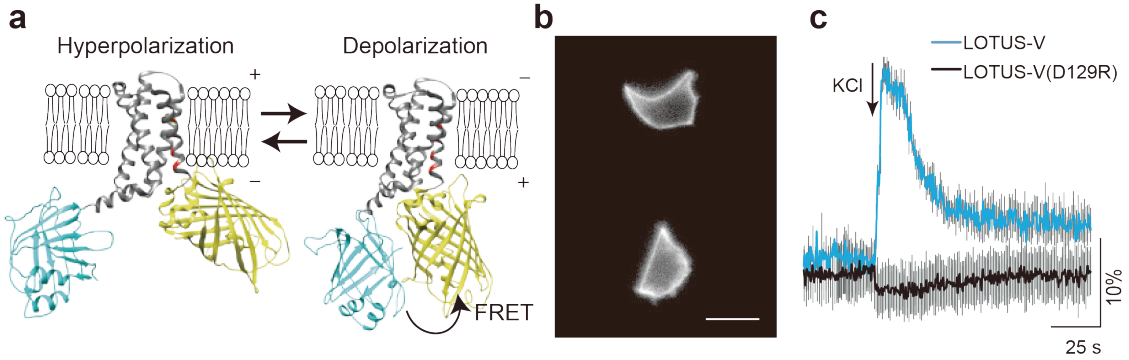

Figure 3 Chemiluminescent voltage indicator, LOTUS-V. (**a**) Molecular design of LOTUS-V (gray; VSD, blue; NanoLuc, yellow; Venus). (**b**) An example chemiluminescent image of GH3 cells expressing LOTUS-V. Scale bar, 20 μm. (**c**) $\Delta R/R_0$ of LOTUS-V (blue) and LOTUS-V (D129R) (black) following 150 mM KCl stimulation. The figure is from reference (17).

LOTUS-V, Wilcoxon rank sum test), and thus named this voltage-insensitive mutant as LOTUS-V(D129R). This result suggests that the signal change shown by LOTUS-V correctly reflects the change in membrane voltage (**Fig.2 and 3c**).

1.4.2. Spectral measurement

Next, I compared the chemiluminescence spectrum of LOTUS-V and LOTUS-V(VenusY66G) preventing chromophore formation of its FRET acceptor (**Fig.4**) (6). Since FRET does not happen in the absence of a functional FRET acceptor, the emission peak at 455 nm derived from NanoLuc emission, was significantly higher than that of LOTUS-V. This result suggests that FRET occurs between the NanoLuc and Venus moieties in LOTUS-V.

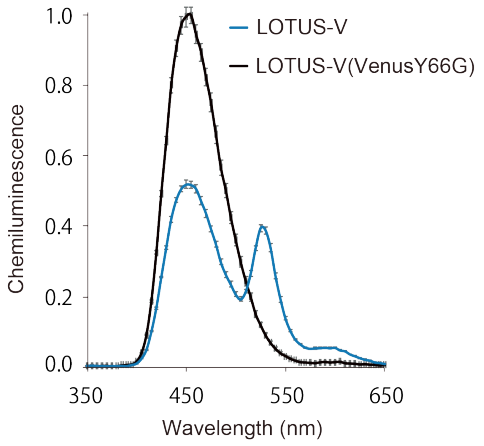

Figure 4 Chemiluminescence spectra of LOTUS-V and LOTUS-V(VenusY66G) in GH3 cells. Gray bars indicate mean ± SE (n=10 trials) at each wavelength. The figure is from reference (17).

1.4.3. Evaluation of substrate cytotoxicity

For further applications of LOTUS-V, cytotoxicity of furimazine, a substrate for NanoLuc moiety, was compared to phototoxicity during fluorescent measurement by a viability assay (**Fig.5**). Many HEK293T cells died 12 h after irradiation cycles

(irradiation for 5 min every 10 min interval) (22 and 100% for 210 and 830 mW/cm^2, respectively), of which power densities were in the typical range for fluorescent voltage recording (14, 16). Fewer dead cells were observed under weaker power density (52 mW/cm^2) or with incubation in 50 μM furimazine (0 and 5%, respectively). While cell proliferation seemed mildly suppressed in the presence of 50 μM furimazine, it is still harmless compared to the excitation light for typical voltage recording.

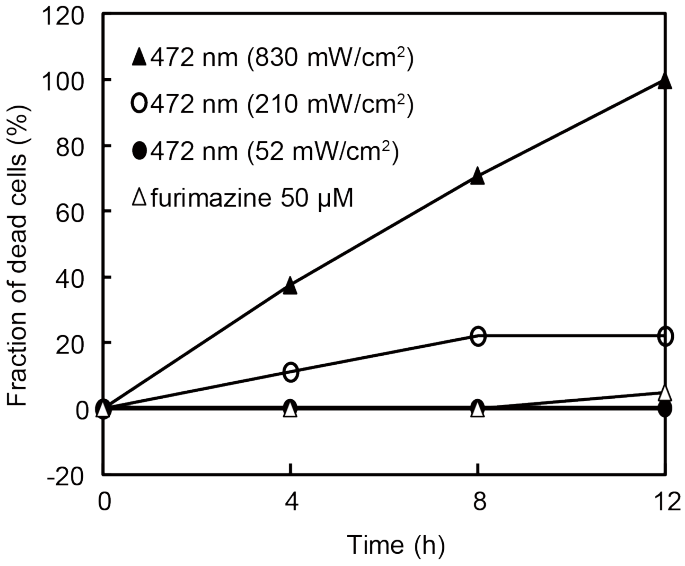

Figure 5 Investigation of furimazine cytotoxicity compared to phototoxicity. HEK293T cells were either irradiated by the excitation light with various intensities (52, 210 or 830 mW/cm^2), or incubated with 50 μM furimazine. Each data point was collected from 60 cells. The figure is from reference (17).

1.5. Perspective

A world-first chemiluminescent voltage indicator, named LOTUS-V was successfully developed by the simple screening method based on KCl-induced depolarization. Previous studies used a path-clamp or field-stimulation method for screening (2, 4, 10, 12), which needs expensive devices and technical electrophysiology knowledge for electrophysiology, while our screening method requires simple KCl addition to the imaging medium. This extremely cheap and easy technique could lower the start-up

hurdle to engineer new GEVIs and be further improved using high throughput screening system with e.g. a microplate reader.

Chapter2 ELECTROPHYSIOLOGICAL CHARACTERIZATION OF LOTUS-V

2.1. Introduction

To know the actual dynamics of membrane voltage from the acquired signal, it is important to quantitatively characterize the performance of GEVIs. While the general focus is how much and how fast a signal changes, typical VSD-based indicators show a sigmoidal response curve against the applied voltages. Thus its half-maximal activation ($V_{1/2}$) and the degree of slope steepness (charged valence) are also important to understand the detection range of the indicator. The application to neural activity recording is particularly demanding, and one might be concerned with whether a GEVI can detect an action potential in neurons, considered to be the minimum unit enabling brain function.

2.2 Purpose and significance

Simultaneous patch-clamp and FRET recordings were performed to precisely know the performance of LOTUS-V and assess whether LOTUS-V can be used for neural activity recording.

2.3. Materials and methods

Gene construction. For oocyte experiments, an *Eco*RI site inside pcDNA3-LOTUS-V was destroyed by PCR mutagenesis using a sense primer (25). Then, the DNA fragment of LOTUS-V (Δ*Eco*RI) was amplified by KOD PCR using a sense primer containing a

Kozak sequence following an *Eco*RI site and a reverse primer containing an *Xba*I site and a stop codon. The DNA fragment for LOTUS-V (Δ*Eco*RI) was ligated between the *Eco*RI and *Xba*I sites of pCS4+-Mermaid2, resulting in pCS4+-LOTUS-V.

For the adeno-associated virus (AAV) expression system, the DNA fragment of LOTUS-V was amplified from pcDNA3-LOTUS-V by KOD PCR using a sense primer containing a Kozak sequence following a *Bgl*II site and a reverse primer containing a *Hin*dIII site and a stop codon. Then it was ligated with pAAV2-hSyn-FlicR1.0 (8, 27) digested by *Bam*HI and *Hin*dIII, resulting in pAAV2-hSyn-LOTUS-V. All constructs were verified by DNA sequencing and the primers are listed in **Table1**.

Electrophysiology and photometry in HEK293T cells and *Xenopus* oocytes. HEK293T cells were cultured in DMEM containing 10% FBS at 37°C in air with 5% CO_2. HEK293T cells were trypsinized and transferred to collagen-coated 35-mm glass-bottom dishes. Next day, pcDNA3-LOTUS-V was transfected into cells by Lipofectamine2000 (Invitrogen), following the manufacturer's protocol. At 23-30 h after transfection, LOTUS-V-expressing cells were subjected to simultaneous FRET and patch-clamp recordings. For characterization, an IX71 inverted microscope (Olympus), equipped with an OrcaFlash 4.0 sCMOS camera (Hamamatsu Photonics), an Axopatch 200B patch clamp amplifier (Axon Instruments), a QE-1RC temperature controller (Warner Instruments) and a RC-41LP coverslip chamber (Warner Instruments) was used. For the bath solution, HEPES-buffered saline (15 mM HEPES, pH 7.4, containing 120 mM NaCl, 2.5 mM KCl, 1.5 mM $MgSO_4$, 2.0 mM $CaCl_2$, 26

mM $NaHCO_3$, 1.1 mM NaH_2PO_4, and 10 mM dextrose) was used. 10 mM HEPES (pH 7.3, adjusted with methanesulfonic acid) for pipette solution included 5 mM NaCl, 10 mM KCl, 10 mM HEPES, 130 mM KOH, 2.5 mM MgATP, 0.3 mM Na_2GTP, and 1 mM EGTA. Chemiluminescence was observed immediately after incubation with 50 μM furimazine and recordings were performed at 30ºC. The images of NanoLuc and Venus channels were acquired sequentially.

LOTUS-V was expressed in *Xenopus* oocytes by a previously described protocol (28). Simultaneous photometry and two-electrode voltage-clamp were conducted using an IX70 inverted microscope (Olympus) and an OC-725C voltage-clamp amplifier (Warner Instruments). The intracellular glass microelectrodes were filled with 2.5 M KCl and the resistance ranged from 0.1 to 3.0 MΩ. The Venus signal was collected with a 20x, NA 0.70 UPlanApo objective lens (Olympus) and detected by a H5784-02 photomultiplier tube (Hamamatsu Photonics). With the use of a 1322A A/D converter (Axon Instruments) and pClamp8 software (Axon Instruments), the output of the optical signal was digitized and stored. The recordings were performed during incubation with 50 μM furimazine.

AAV preparation. The AAV vector was prepared as described previously with some modifications (29). Briefly, equal amounts of pAAV2-hSyn-LOTUS-V, pAAV-DJ (30), and pHelper (Cell Biolabs, INC.) plasmids were co-transfected into HEK293T cells by the $FuGENE_{HD}$ transfection reagent (Promega), following the manufacturer's protocol. Cells were trypsinized and centrifuged for 5 min at 1,000 rpm at 4ºC at 3 days

post-transfection. After that, the cell pellet was resuspended in 200 μl HEPES-buffered saline (10 mM HEPES, pH 7.3, containing 150 mM NaCl, 2.5 mM KCl, 1M $MgCl_2$, 1M $CaCl_2$). Then the suspension was subjected to three freeze-and-thaw cycles. It was incubated in a water bath with 1 μl of benzonase nuclease at 45ºC for 15 min, and centrifuged for 10 min at 16,000 *g* at 4ºC twice to remove cell debris. Aliquots were stored at -80ºC until used.

Rat hippocampal neuron culture and imaging. Primary cultures of hippocampal neurons and astrocytes were prepared from Sprague-Dawley rats (embryonic day 17). The cells were dissociated in Hanks' Balanced Salt solution (HBSS) (Wako) containing 1mM HEPES and 100 U/ml penicillin/streptomycin, and were mounted onto a poly-L-lysine (Sigma) coated 35-mm dish at the density of 3.5×10^4 cells/12-mm-diameter coverslip. At 5 h post-plating, the medium was exchanged for Neuro Basal medium (Thermo Fisher) including 2% L-glutamine and B27 (Invitrogen). The cells were incubated in 5% CO_2 at 37°C. Half of the culture medium was replaced with fresh medium on day 7 *in vitro* (DIV-7). On DIV-14, the culture was incubated with the stock solution of AAV vector at 1.0×10^{10} TU/ml for 5 h. Experiments were carried out at 7–10 days after infection.

Electrophysiology and photometry in hippocampal neurons. LOTUS-V-expressing neurons were subjected to simultaneous FRET and patch-clamp recordings at 7–10 days post-infection. The culture medium was replaced with HBSS (Gibco) containing 5.5

mM D-Glucose and 20 mM HEPES (pH 7.2), and the dish was set on the stage of an Axiovert 200M inverted microscope (Carl Zeiss). With the use of an Axoclamp 200B patch-clamp amplifier with a capacitive headstage (Axon Instruments) and glass recording electrodes (3–5 MΩ), Patch-clamp recordings in the whole-cell mode were performed. The electrodes were filled with intracellular solution (140 mM potassium gluconate, 1 mM $MgCl_2$, 5 mM KCl, 2 mM Mg-ATP, 0.1 mM EGTA, 5 mM HEPES, adjusted to pH 7.2 with KOH). Whole-cell recordings were low-pass-filtered at 1 kHz and digitized at 10 kHz with a Digidata 1342 digitizer (Axon Instruments) and AxoClamp 9.0 software (Axon Instruments). Chemiluminescence of LOTUS-V was observed by incubation with 50 μM furimazine (Promega). The recordings were carried out at 23ºC. Chemiluminescence signal was measured with a MiCAM Ultima-L CMOS camera (Brain Vision), a C8600-05 GaAsP image intensifier unit (Hamamatsu Photonics) and W-VIEW GEMINI image splitting optics (Hamamatsu Photonics). A FF509-FDi01-25×36 dichroic mirror (Semrock) and no emission filters were installed into the image splitting optics.

Data analysis All of the imaging data were processed by Fiji, BrainVision analyzer software and R-software (Version 3.2.2.). Curve fitting was performed via Origin 8.5.1 (OriginLab).

For fitting the voltage sensitive curve, the following Boltzmann function was used;

$$\frac{\Delta R}{R_0} = \frac{C_1}{1+\exp(\frac{Ze(V-V_{1/2})}{kT})} + C_2$$

where Z is the effective valence; e is the elementary electric charge; $V_{1/2}$ is the voltage at which $\Delta R/R_0$ is half-activated; k is the Boltzmann constant; T is the temperature in Kelvin; C_1 and C_2 are constant values;. For the analysis of voltage kinetics, the activation and deactivation curves of $\Delta R/R_0$ were fitted by the following two-component exponential equation;

$$\frac{\Delta R}{R_0} = C_3 \exp(\frac{t-t_0}{\tau_1}) + C_4 \exp(\frac{t-t_0}{\tau_2}) + C_5$$

where t_0 is the initial time point; τ_1 and τ_2 are the time constants for the fast and slow components; and C_3, C_4, C_5 are the constant value (C_3 and C_4 were used to calculate the fraction of τ_{fast}).

2.4. Results and discussion

2.4.1. Characterization in HEK293T cells and *Xenopus* oocytes

To quantitatively characterize the properties of LOTUS-V, FRET recording was performed in LOTUS-V-expressing HEK293T cells and stepwise changes in membrane voltage were simultaneously applied. The intensity in Venus and NanoLuc channels reciprocally changed depending on the applied voltage (**Fig.6a**). From this data, $\Delta R/R_0$ was calculated and the plots were fitted by Boltzmann function. The analysis revealed the dynamic range; 21.0±0.9%/100 mV [mean ± SE] (n=5 cells), the effective valence; 0.5, and $V_{1/2}$; -11 mV (**Fig.6b**).

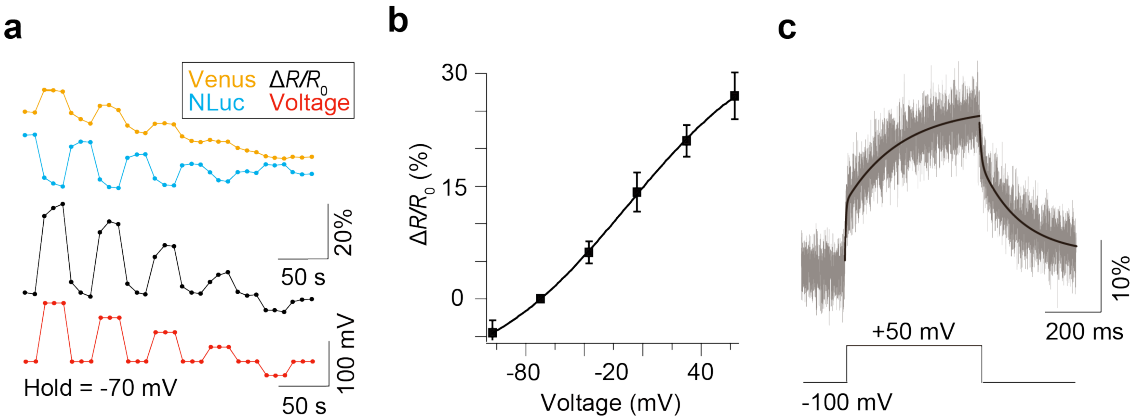

Figure 6 Electrophysiological characterization in HEK293T cells (a-b) and *Xenopus* oocytes (c). (**a**) The Venus, NanoLuc signals ($\Delta L/L_0$; yellow and blue, respectively), and $\Delta R/R_0$ (black) against stepwise voltage changes (+63, +30, +4, −37 and −107 mV, respectively) from a holding voltage (−70 mV; red) in a HEK293T cell. (**b**) Plots of the fractional $\Delta R/R_0$ versus the applied membrane voltages. Error bars indicate mean ± SD (n=5 cells). The curved line indicates a Boltzmann function. (**c**) The $\Delta L/L_0$ in the Venus signal in response to the voltage change (+50 mV) from the holding voltage (−100 mV) in *Xenopus* oocytes (n=6 cells). The black curved line indicates the result of two-component exponential curve fitting. The figure is from reference (17).

To confirm the voltage sensitivity in a different cell type, the response kinetics against the applied voltage was confirmed in *Xenopus* oocytes and fitted by two-component exponential equation after data acquisition at 5 kHz with off-line time averaging of 32 sweeps and Bessel filtering at 1 kHz (**Fig.6c**). For the activation curve (from -100 mV to +50 mV), time constants of the fast and slow components were 3.09 ms (fraction, 37.3%) and 204 ms, respectively. For the deactivation curve (from +50 mV to -100 mV), those were 6.12 ms (fraction, 29.4%) and 144 ms, respectively.

2.4.2. Characterization in primary hippocampal neuron culture

To confirm the utility of LOTUS-V in neurons, it was expressed in primary cultures of rat hippocampal neurons via AAV-mediated expression. Signal change during patch-clamp recording was investigated (**Fig.7**). By addition of furimazine, intense chemiluminescence was observed from a single neuron (**Fig.7a**), and the signal could be recorded at 1 kHz frame rate. As observed in HEK293T cells, LOTUS-V had a wide detectability range in neurons (the detection range; -120 to +80 mV, the dynamic range; 7.6±0.2%/+200 mV [mean ± SE] n=4 cells, the charged valence; 0.7, and $V_{1/2}$; -45.5 mV) (**Fig.7b**), suggesting that it should detect both subthreshold activity and an action potential. Next, response kinetics of LOTUS-V in neurons was investigated (**Fig.7c**). For the activation curve (from -70 mV to +30 mV), time constants of the fast and slow components were 18.4 ms (fraction, 54.3%) and 238.8 ms, respectively. For the deactivation curve (from +30 mV to -70 mV), those were 15.2 ms (fraction, 37.8%) and 108.4 ms, respectively. Also, during the action potential, a significant signal change was observed (**Fig.7d**).

Compared with recently published GEVIs, the dynamic range in HEK293T cells and hippocampal neurons is comparable (7, 8, 14). Also the time constants of LOTUS-V are similar values to those of the widely used GEVI, called ArclightQ239 (3, 31), suggesting that LOTUS-V is expected to be useful for voltage imaging in various cell types.

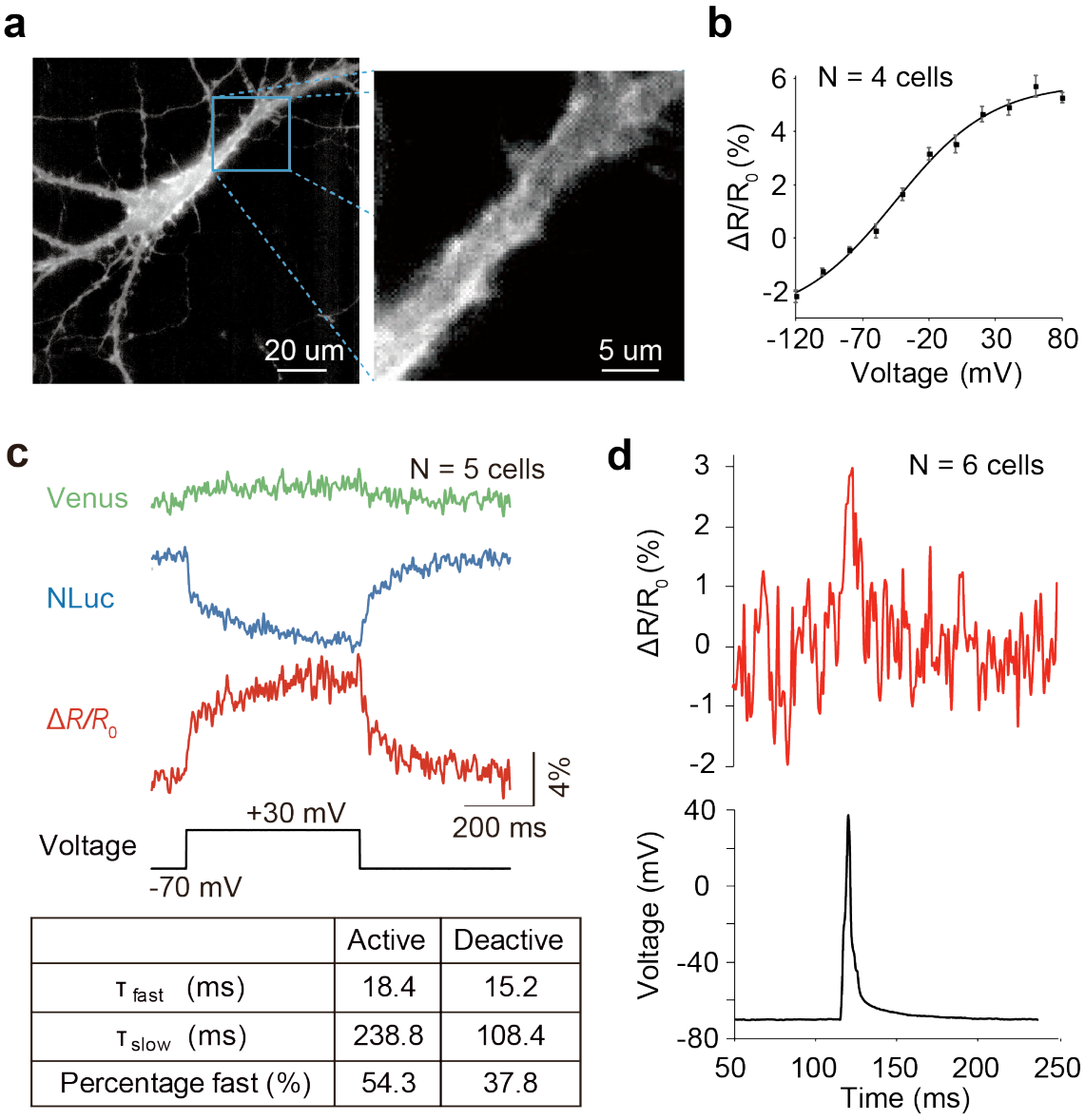

	Active	Deactive
τ_{fast} (ms)	18.4	15.2
τ_{slow} (ms)	238.8	108.4
Percentage fast (%)	54.3	37.8

Figure 7 Electrophysiological characterization in hippocampal neurons. (**a**) An example chemiluminescence image of a hippocampal neuron expressing LOTUS-V. (**b**) Plots of fractional $\Delta R/R_0$ against voltage changes (n=4 cells). They were fitted by a Boltzmann function (black line). (**c**) The Venus and NanoLuc signals ($\Delta L/L_0$; green and blue, respectively), and $\Delta R/R_0$ in response to the applied voltage (-70 mV to +30 mV, n=5 cells). (**c**; table) The fast and slow components, and their fraction of time constant. The activation and deactivation curves of $\Delta R/R_0$ were fitted by a two-component exponential equation. (**d**) (upper) Action potential waveform of $\Delta R/R_0$ and (lower) electrophysiology (n=6 cells). The frame rate was 1 kHz. Error bars indicate mean ± SE. The figure is from reference (67).

2.5. Perspective

While the performance of LOTUS-V was verified in HEK293T cells, *Xenopus* oocytes and primary culture of hippocampal neurons, it has still room for improvement. One issue to be addressed in future is relatively small dynamic range in neurons, which is also seen in other GEVIs (7, 32). Since the membrane composition and the efficiency of membrane trafficking can differ depending on cell type (16), screening of GEVI should be conducted in neurons if one attempts to optimize it for neural activity recording. Another issue is the relatively slow response kinetics of LOTUS-V. Recently published GEVIs show faster kinetics (a few tens of ms) (4, 10, 14, 31) mainly because of a different mechanism for voltage sensing. An idea to improve kinetics of LOTUS-V is to use the paradigm of ASAP1(4), which consists of a VSD from Gg-VSP and cpGFP inserted into S3-S4 loop of VSD. If cpNanoLuc could be inserted into S3-S4 loop of VSD without any stractual hinderance, the chemiluminescent GEVI should have faster kinetics.

Chapter3 *IN VITRO* DRUG EVALUATION

3.1. Introduction

Human-induced pluripotent stem cells (hiPSCs) were developed by introducing Oct3/4, Sox2, Kif4 and c-Myc genes into fibroblasts and can be ideally differentiated into any cell type (33). Importantly, hiPSCs can be made from differentiated somatic cells, and thus overcome problems regarding the ethics, associated with use of human-embryonic stem cells (hESCs) (34). Recently, cardiomyocytes derived from hiPSCs (hiPSC-CMs) have gained attention as a platform for personalized drug screening *in vitro* (35). In cardiology, it is well known that an abnormal duration between the start of Q wave and the end of T wave (QT interval) on an electrocardiogram reflects various disease states (36). Since the QT interval corresponds to action potential duration (APD), drug effect can be investigated by GEVIs (35). However, these techniques rely on fluorescent excitation which are not free from photobleaching or phototoxicity, and thus long-term measurements were not shown. Also, hiPSC-CMs move when they contract, motion artifact is a major concern for genuine quantitative measurements using intensiometric indicators.

3.2. Purpose and significance

LOTUS-V was expected to have several advantages over other GEVIs in iPSC-CMs, such as high signal-to-background ratio (SBR) owing to absense of autofluorescence, negligible photobleaching and phototoxicity, and mitigation of motion artifact by ratiometry. Therefore, I expected that LOTUS-V could quantitatively assess drug effect

on hiPSC-CMs for extended periods of time.

3.3. Materials and methods

Gene construction. For the lentiviral expression system, an *Xho*I site inside pcDNA3-LOTUS-V was destroyed by PCR mutagenesis using a sense primer (25). Then, the DNA fragment of LOTUS-V(Δ*Xho*I) was amplified by KOD PCR using a sense primer containing a Kozak sequence following a *Bgl*II site and a reverse primer containing an *Xho*I site and a stop codon. CS-CDF-LOTUS-V-PRE was created by ligating LOTUS-V (Δ*Xho*I), EF1α and CS-CDF-EG-PRE digested by *Eco*RI and *Xho*I. In this process, an *Age*I site following the EF-1 promoter was replaced with a *Bam*HI site. To construct CS-CDF-Mermaid2-PRE and CS-CDF-VSFP-BF1.2-PRE, the In-Fusion HD Cloning Kit (Clontech) was used, following the manufacturer's protocol. To construct CS-CDF-ArclightQ239-PRE, the DNA fragment of ArclightQ239 [Addgene: Plasmid #36856] was amplified by KOD PCR using a sense primer containing a *Bgl*II site and a Kozak sequence, and a reverse primer containing an *Xho*I site and a stop codon. Then, it was replaced with Mermaid2 from CS-CDF-Mermaid2-PRE. All constructs were verified by DNA sequencing and the primers are listed in **Table 1**.

Preparation of lentivirus. Equal amounts of CS-CDF-LOTUS-V-PRE (or other constructs of a fluorescent GEVI), pCAG-HIVgp, and pCMV-VSV-G-RSV-Rev were transfected into HEK293T cells by FuGENE HD transfection reagent (Promega),

following the manufacturer's protocol. At 3 days post-transfection, the culture medium was collected and the viruses were harvested with a Lenti-X concentrator (Takara), following the manufacturer's protocol. The virus titer was adjusted to 1.0×10^7 Infectious units (IFU)/ml measured by Lenti-X GoStix (Takara).

PC12 cell culture pheochromocytoma (PC12) cells (ATCC, CRL-1721) were grown in DMEM containing 10% HS and 5% FBS at 37°C in air with 5% CO_2. The cells were placed on homemade 35-mm glass-bottomed dishes coated with 0.04% polyethyleneimine 4 days before imaging. At the same time, the cells were incubated with lentivirus vector (1.0×10^5 IFU/ml) for expression.

hiPSC-CMs culture and imaging. The aggregates of hiPSC-CMs (ReproCardio2, ReproCell) were prepared following the manufacturer's protocol with some modifications. Briefly, the cells were transferred to 96-well round-bottomed plates to induce aggregation and incubated with lentivirus vector (1.0×10^5 IFU/ml) at day 0 *in vitro* (DIV0). At DIV3, the aggregates were transferred to 96-well flat-bottomed plates coated with ReproCoat to induce the process of cardiac maturation. At DIV2 and DIV4-10, half of the culture medium was replaced with ReproCardio Culture Medium 2, containing 20% FBS and 1% Penicillin/Streptomycin.

Imaging was carried out at DIV8-10 using an Eclipse Ti-E inverted microscope equipped with a 20x, NA 0.7, Plan Fluor objective (Nikon). LOTUS-V chemiluminescence was induced with 50 μM furimazine and was separated by a

W-VIEW GEMINI A12801-01 image splitting optics (Hamamatsu Photonics) equipped with a FF509-Di01-25×36 dichroic mirror (Semrock) and no emission filters. Chemiluminescence was recorded by an iXon3 EMCCD camera (Andor Technology) under the control of MetaMorph software (Molecular Devices). Camera binning was set at 2 and 16 for a movie and the analysis, respectively and the temperature was kept at 37°C by an iNUG2 stage top incubator (Tokai Hit) during imaging. For long-term imaging, fresh medium containing 50 μM furimazine was continuously perfused by a MP-1000 peristaltic pump (EYELA).

Voltage imaging with fluorescent indicators. Voltage imaging was carried out using an Eclipse Ti-E inverted microscope equipped with a 20x, NA 0.7, Plan Fluor objective (Nikon) and an iXon Ultra EMCCD camera (Andor Technology). To measure the signal of Mermaid2, a FF01-438/24-25 excitation filter and a FF458-Di02-25×36 dichroic mirror (Semrock) were used. The fluorescence signal was split by a W-VIEW GEMINI A12801-01 image splitting optics (Hamamatsu Photonics) equipped with FF01-483/32-25 and FF01-525/45-25 emission filters (Semrock). For VSFP BF1.2, a FF01-500/24-25 excitation filter, a FF520-Di02-25×36 dichroic mirror (Semrock) were used. A FF580-FDi01-25×36 dichroic mirror, FF01-542/27-25 and FF01-624/40-25 emission filters (Semrock) were installed to the image splitting optics. For ArclightQ239, a FF02-472/30-25 excitation filter, a FF495-Di03-25×36 dichroic mirror and a FF01-520/35-25 emission filter (Semrock) were used.

Voltage imaging with Di-8-ANEPPS. Before imaging, 40 μM Di-8-ANEPPS (Invitrogen) was loaded into hiPSC-CMs in ReproCardio assay medium (ReproCell) for 10 min. A FF01-438/24-25 excitation filter, a FF458-Di02-25×36 dichroic mirror (Semrock) were used. The fluorescence signal was split by the image splitting optics equipped with a FF562-Di03-25×36 dichroic mirror, FF01-537/26-25 and FF01-593/LP-25 emission filters (Semrock).

Data analysis To calculate the drop (D) of the $\Delta R/R_0$ signal from 0 h to 1 h, the following equation was used;

$$D(\%) = \frac{((\frac{\Delta R}{R_0})_{0h} - (\frac{\Delta R}{R_0})_{1h})}{(\frac{\Delta R}{R_0})_{0h}} \times 100$$

where $(\Delta R/R_0)_{0h}$ and $(\Delta R/R_0)_{1h}$ were $\Delta R/R_0$, 0 h and 1 h after initiation of the experiment, respectively. APD_{90} was calculated by measuring the duration at 90% of maximal activation of spikes.

3.4. Result and discussion

3.4.1 Comparison of LOTUS-V and a voltage-sensitive dye

To perform voltage imaging in hiPSC-CMs, LOTUS-V was expressed via lentivirus-mediated expression. During spontaneous contraction, the emission ratio of LOTUS-V increased, reflecting the action potential of cardiomyocytes (**Fig.8a-b**). The action potential morphology closely resembled that of Di-8-ANEPPS (**Fig.8b**), a

commonly used voltage-sensitive dye (35, 37), although some high frequency components were lost. Also action potential duration (APD_{90}) measured by LOTUS-V and Di-8-ANEPPS was linearly correlated (R^2 = 0.87) (**Fig.8c**), suggesting that quantitative evaluation based on APD_{90} can be performed with LOTUS-V.

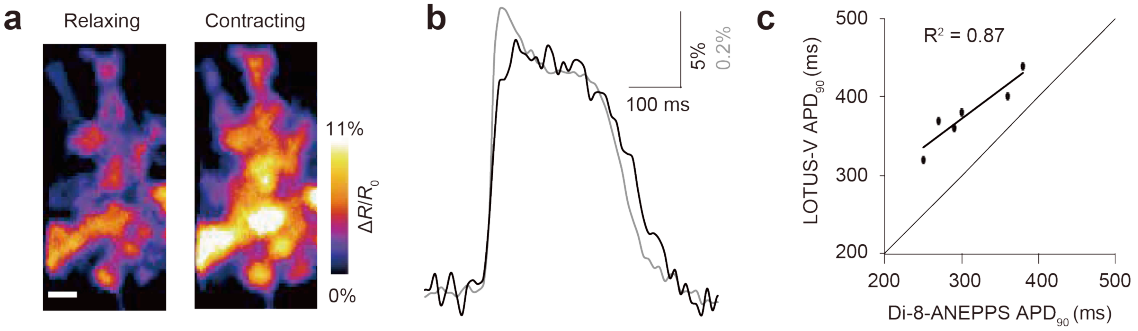

Figure 8 Voltage recording using LOTUS-V in hiPSC-CMs. (**a**) Example images showing $\Delta R/R_0$ in relaxed and contracted states (n=23 spikes). Scale bar, 50 μm. (**b**) Action potential morphology taken by LOTUS-V (black) and Di-8-ANEPPS (gray) during contraction (n=38 spikes). The power density of excitation light for fluorescence imaging was 735 mW/cm^2. (**c**) Correlation between APD_{90} measured by LOTUS-V and Di-8-ANEPPS. The thick black line indicates least squares fitting. The figure is from reference (17).

3.4.2. Evaluation of signal-to-background ratio

SBR is a ruler to evaluate how sensitively a signal can be detected. Usually in thick specimens, strong autofluorescence from naturally existing chromophores, such as nicotinamide adenine dinucleotide phosphate (NADPH) and flavin significantly reduces the SBR of an acquired image, which is often problematic in fluorescent voltage imaging. To test the applicability of LOTUS-V in that situation, SBR of LOTUS-V and ArclightQ239, a GEVI used in cardiology and neuroscience research (16, 37), was

compared in thin (PC12 cells) and thick (hiPSC-CMs aggregates) samples (**Fig.9**).

During voltage recording, the SBR of LOTUS-V was always similar in PC12 cells and hiPSC-CMs. On the other hand, SBR of ArclightQ239 was significantly reduced in hiPSC-CMs aggregates (**Fig.9**). This result demonstrates that chemiluminescence imaging is highly robust against variation in sample thickness, while the SBR of fluorescence imaging significantly depends on minimising it.

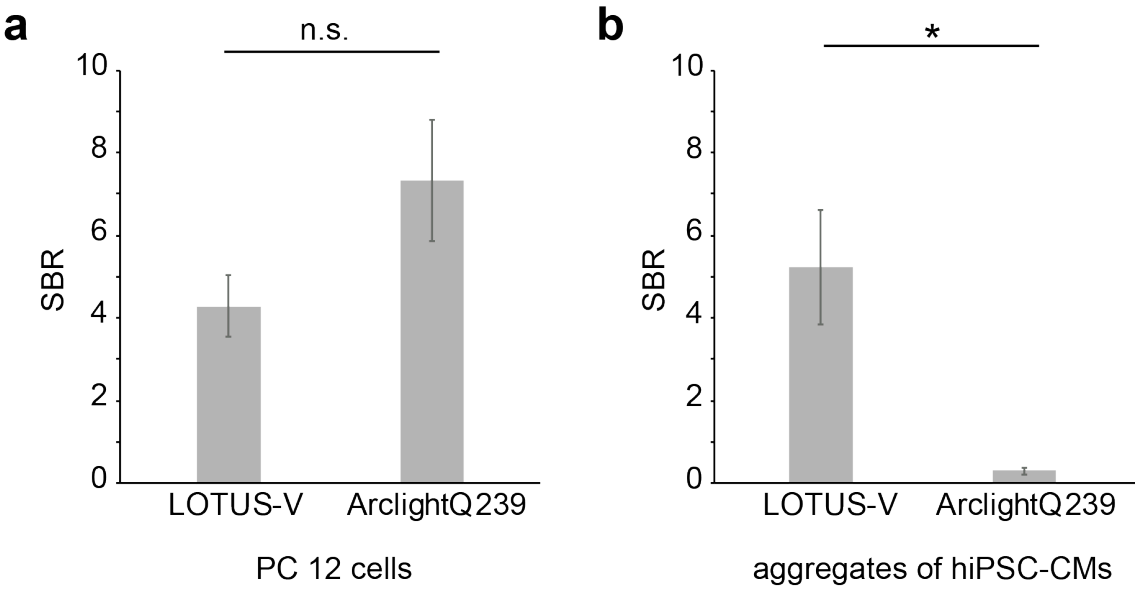

Figure 9 Comparison of SBR of LOTUS-V and ArclightQ239. SBR of LOTUS-V and ArclightQ239 (**a**, in PC12 cells, 4.29±0.74 and 7.32±1.45, respectively; n=5 cells, n.s.; **b**, in hiPSC-CMs, 5.23±1.39 and 0.31±0.09, respectively n=5 aggregates, $p<0.05$, Wilcoxon rank sum test). For fair comparison with ArclightQ239, the Venus signal from LOTUS-V was used to calculate its SBR. Error bars indicate mean ± SE. n.s.; not significant, *; $p<0.05$. The figure is from reference (17).

3.4.3. Evaluation of motion artifact

Motion artifact is a critical issue to quantitatively analyze changes in moving specimens. To confirm whether LOTUS-V can sufficiently mitigate the motion artifact by ratiometry, the signal of LOTUS-V, LOTUS-V(D129R) (a negative control for ratiometry), EGFP (a negative control for intensiometry) and ArclightQ239 (an intensiometric voltage indicator) was measured inside and at the periphery of hiPSC-CMs aggregates, respectively (**Fig.10**).

As expected, the spike morphology of ArclightQ239 in the different regions was inconsistent (**Fig.10a**). Also local fluorescence intensity of EGFP alone changed depending on the direction of contraction (**Fig.10b**), suggesting that experiments using intensiometric GEVIs are not appropriate for quantitative measurement in hiPSC-CMs

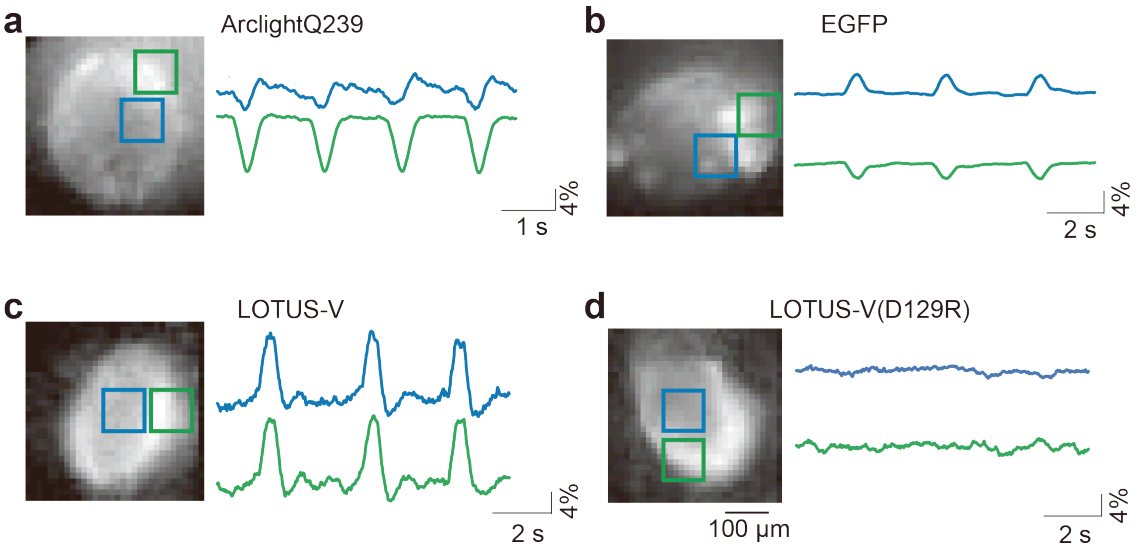

Figure 10 The effect of motion artifact (**a-d**) The signal from (**a**) ArclightQ239, (**b**) EGFP, (**c**) LOTUS-V and (**d**) LOTUS-V(D129R) in the different ROI (blue and green) located at hiPSC-CMs. The signals were processed by the moving average (window length of 20 frames). The figure is from reference (17).

aggregates. Conversely, while LOTUS-V(D129R) showed no signal changes (**Fig.10d**), the spike morphology of LOTUS-V was almost identical in the different regions (**Fig.10c**). This result suggests that the signal of LOTUS-V was free from motion artifacts and reflected actual changes in membrane voltage independent of movement.

3.4.4. Long-term voltage imaging

Although the NanoLuc signal is known to decay with a half-life over 2 h due to substrate consumption (24), imaging using LOTUS-V is usually limited to 30 min to obtain the data with similar SBR, which is important to standardize results for subsequent comparison (e.g. drug). To detect action potentials over extended period, LOTUS-V-expressing hiPSC-CMs were perfused with medium supplemented with furimazine, and the result compared with that obtained by fluorescence measurement (**Fig.11**). While the upstroke peak amplitude of VSFP BF1.2 and Mermaid2

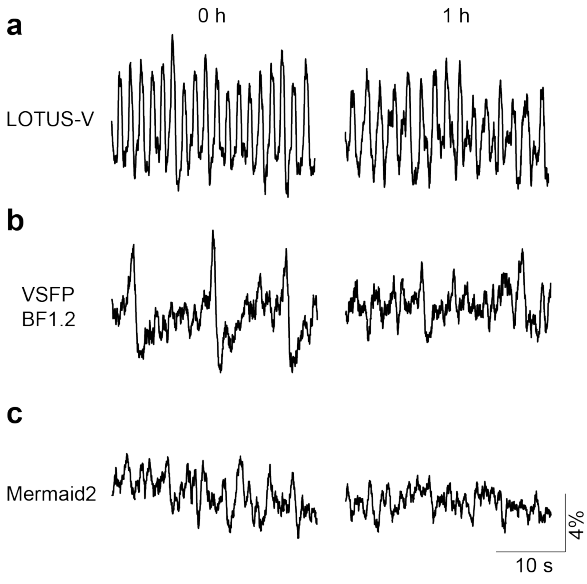

Figure 11 Long-term recording. The signals of (**a**) LOTUS-V, (**b**) VSFP BF1.2, and (**c**) Mermaid2 at (left) 0 h and (right) 1 h. hiPSC-CMs were perfused with the medium supplemented with furimazine. Excitation light for VSFP BF1.2 (44.9 mW/cm^2) and Mermaid2 (34.8 mW/cm^2) was applied continuously. The signals were processed by the moving average (window length of 20 frames). The figure is from reference (17).

significantly reduced after 1 h (($\Delta R/R_0)_{0h}$, 7.01±0.20% and 2.07±0.20% [mean ± SE]; $(\Delta R/R_0)_{1h}$, 3.58±0.73% and 0.59±0.08%; $p<0.05$ and 0.01; decreasing rate, 48.9% and 78.3%, respectively; n=5 sessions, Wilcoxon rank sum test), LOTUS-V maintained almost consistent detectability (($\Delta R/R_0)_{0h}$, 7.61±0.17%; $(\Delta R/R_0)_{1h,}$ 6.82±0.27% [mean ± SE]; n.s.; decreasing rate, 10.3%; n=5 sessions, Wilcoxon rank sum test). This result demonstrated that the continuous supplement of additional substrate enables long-term recording using LOTUS-V.

Interestingly ArclightQ239 kept unchanged detectability of action potentials for 1 h (**Fig.12**; $(\Delta F/F_0)_{0h}$, -6.74±0.06%; $(\Delta F/F_0)_{1h,}$ -6.62±0.08% [mean ± SE]; n.s.; decreasing rate, 1.7%; n=5 sessions, Wilcoxon rank sum test), but its spike varies within aggregates, and thus the obtained signal does not reflect actual voltage dynamics. (**Fig.10**).

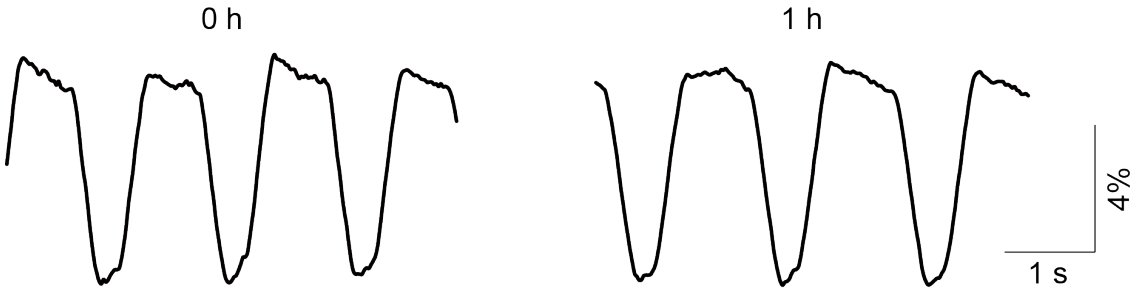

Figure 12 Long-term imaging using ArclightQ239. The signal of ArclightQ239 at 0 h and 1 h. Excitation light (2.84 mW/cm^2) was irradiated continuously. The signal was processed by the moving average (window length of 20 frames). The figure is from reference (17).

3.4.5. Evaluation of spike morphology upon drug application

Next, I investigated whether LOTUS-V can distinguish the change in electrophysiological state induced by various chemicals. Since hiPSC-CMs behave heterogeneously (38), the same cell populations before and after drug application were compared to minimize the impact of variability in the cells themselves.

Spike frequency increased after adding isoproterenol (ISO), which is a non-selective β-adrenergic agonist often used to treat bradycardia (**Fig.13a**) (39). Also tetrodotoxin (TTX), which is a sodium channel blocker, shortened APD and reduced the

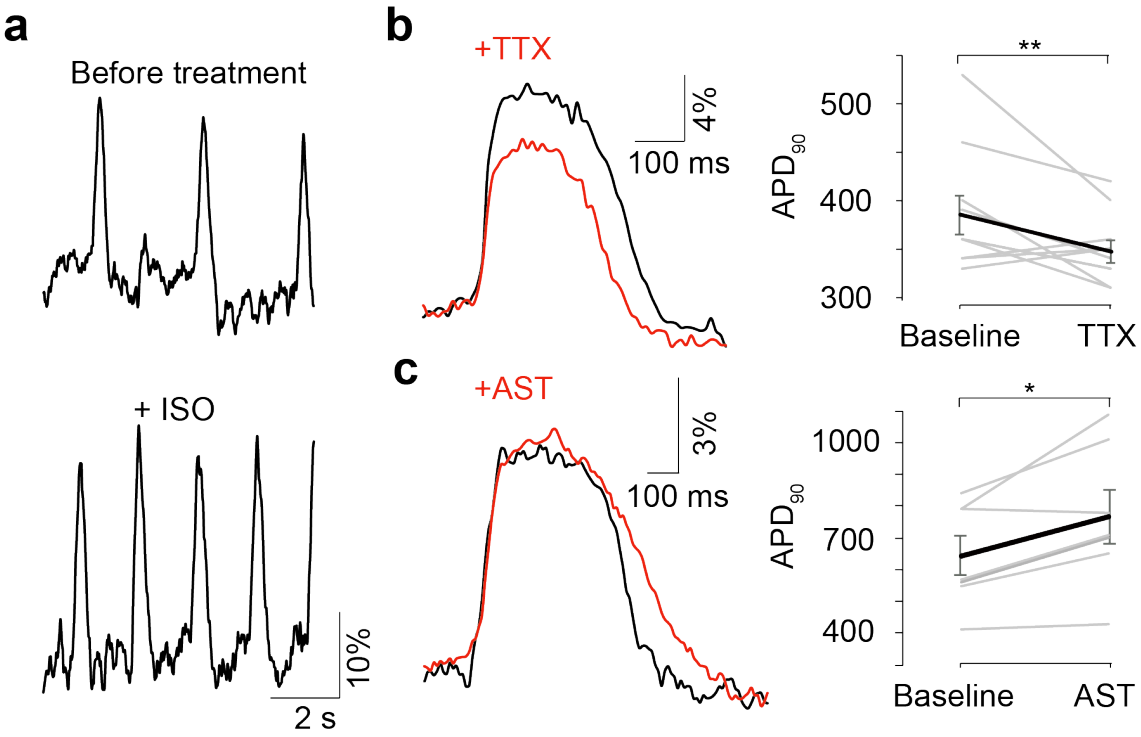

Figure 13 Evaluation of drug effect. (**a**) The LOTUS-V signal before and after adding 100 nM isoproterenol. (**b,c**) Action potential morphology before and after adding (**b**) 30 μM TTX (n=10) and (**c**) 10 μM astemizole (n=7). The right graphs indicate the change in APD_{90} after drug addition. Wilcoxon signed-rank test was performed. Error bars indicate mean ± SE. *; $p<0.05$, **; $p<0.01$. The figure is from reference (17).

peak amplitude as previously reported (40) (**Fig.13b**; APD_{90}, 387±20 ms reduced to 350±11 ms [mean ± SE] following TTX; $\Delta R/R_0$, 13.2±0.6% falls to 10.9±0.4% following TTX; $p<0.01$ and $p<0.05$, respectively; n=10 aggregates, Wilcoxon signed-rank test). Finally, astemizole (AST), which is a human ether-a-go-go-related (hERG) channel blocker, extended APD_{90} (41) (**Fig.13c**; APD_{90}, 644±61 ms to 767±84 ms [mean ± SE]; $p<0.05$; n=7 aggregates, Wilcoxon signed-rank test). These results clearly suggest that LOTUS-V could assess drug effect in hiPSC-CMs, based on not only spike frequency but also the spike morphology.

3.5. Perspective

Collectively, LOTUS-V has been shown to enable sensitive and long-term imaging even in thick spontaneously contracting aggregates of hiPSC-CMs, where autofluorescence and motion artifact are problematic. Thus, it opens the door for quantitative and long-term drug evaluation, an important step toward the unmet need for chronic pharmacological toxicity testing.

Although I demonstrated the advantages of chemiluminesce imaging using LOTUS-V, the response speed of LOTUS-V seems a bottleneck to quantitatively analyze high frequency domain in an action potential (**Fig.8b**). To investigate it, another chemiluminescent voltage indicator which has faster kinetics might need to be developed with the effort as discussed in the chapter "Characterization by electrophysiology."

At this time, imaging of hiPSC-CMs was conducted one by one, however higher

throughput imaging systems are necessary particularly for drug discovery and medical usage. Currently, high throughput drug screening systems based on a plate reader are commercially available (e.g. FDSS/μCELL Functional Drug Screening System, Hamamatsu Photonics). Although convenient for high throughput drug screening in cardiomyocytes, GEVIs have not been applied to it so far, mainly because of their low SBR. Since excitation light is irradiated to wide field of view (i.e. not concentrated to the specimen) for simultaneous imaging in multiple wells, low SBR of fluorescent voltage indicator is problematic. Conversely, LOTUS-V offers much higher SBR, and thus high throughput drug screening system based on a plate reader seems an ideal partner for it.

Chapter4 *IN VITRO* OPTOGENETIC STIMULATION

4.1. Introduction

Optogenetics allows us fast and reversible manipulation of neural activity has revolutionized current neuroscience. ChR2 is a light-driven cation channel able to depolarize membrane voltage (18). On the other hand, Halorhodopsin (eNpHR) (42) and ArchaerhodopsinT (ArchT) (11), which are light-driven chloride and proton pumps respectively, can hyperpolarize membrane voltage. These tools enable bidirectional control of neural activity by light irradiation and are indispensable in the field of neuroscience, promising to extend our knowledge of brain function in conjunction with GEVIs.

"All-optical electrophysiology", the technique in which voltage imaging is combined with optogenetic manipulation has been proposed (8, 10). However, this technique requires carefully selected partners to prevent unintended activation of the optogenetic actuator by excitation light for voltage imaging. To make matters worse, for example, if ChR2(H134R) (18) and eNpHR3.0 (42) are expressed in cells for bidirectional optical control, the composite absorption spectrum ranges from 350 to 650 nm (**Fig.14**). Since the wavelength of excitation light for all GEVIs are within this range, simultaneous voltage imaging with unrestricted optogenetic manipulation is impossible with current techniques for voltage imaging.

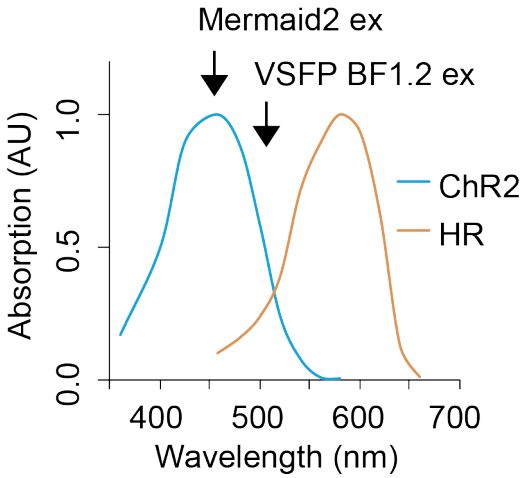

Figure 14 Overlay absorption spectra of ChR2(H134R) (blue) and eNpHR3.0 (yellow). The arrows show the excitation peak of VSFP BF1.2 and Mermaid2. The figure is from reference (17).

4.2. Purpose and significance

Since voltage imaging with LOTUS-V does not need excitation light and chemiluminescence intensity is expected to be much lower than the intensity threshold of the half maximal activation of optogenetic actuators (43), simultaneous voltage imaging with unrestricted optogenetic stimulation should be possible.

4.3. Materials and methods

Gene Construction. To express ChR2(H134R) and eNpHR3.0 equally in cells, the self cleaving P2A peptide (44) was inserted between them. First, each synthesized oligonucleotide was annealed to make the DNA fragment of P2A peptide. Then, it was inserted between the *Eco*RI and *Not*I sites of pcDNA3. The DNA fragment of ChR2(H134R) (Addgene: Plasmid #20945) was amplified by KOD PCR using a sense primer containing a *Not*I site and a reverse primer containing a stop codon and an *Xba*I site. Then, it was subcloned into pcDNA3-P2A digested by *Not*I and *Xba*I. Subsequently, the DNA fragment of eNpHR3.0 (Addgene: Plasmid#26966) was

amplified by KOD PCR using a sense primer containing a Kozak sequence following a *Hin*dIII site, and a reverse primer containing an *Eco*RI site. Then, it was subcloned into pcDNA3-P2A-ChR2(H134R) digested by *Hin*dIII and *Eco*RI. To construct CS-CDF-QuasAr2-PRE, the DNA fragment of QuasAr2 [Addgene: Plasmid #51694] was amplified by KOD PCR using a sense primer containing a Kozak sequence following a *Bgl*II site, and a reverse primer containing a stop codon and an *Xho*I site. Then it was replaced with Mermaid2 of CS-CDF-Mermaid2-PRE. All of the constructs were verified by DNA sequencing and the primers are listed in **Table 1**.

Cell culture. PC12 cells were cultured as described in chapter 3. 12 h after transferring the cells to 35-mm glass bottom dishes, equal amount of the plasmids encoding a GEVI and eNpHR3.0-P2A-ChR2(H134R) was transfected into PC12 cells with Lipofectamine 2000 (Invitrogen), following the manufacturer's protocol. 4-6 h after transfection, the medium was replaced with new one containing 100 ng/ml nerve growth factor (NGF) (Promega). The cells were incubated to induce neuron-like differentiation and imaging was conducted 3-4 days after transfection. HEK293T cell culture and transfection with Lipofectamine 2000 were performed as described above.

Voltage imaging with optogenetic actuators. Imaging was carried out using an Eclipse Ti-E inverted microscope equipped with a 40x, NA 1.30, Plan Fluor oil-immersion objective (Nikon) and an iXon Ultra EMCCD camera (Andor Technology). For LOTUS-V, W-VIEW GEMINI A12801-01 image splitting optics

(Hamamatsu Photonics) equipped with a FF509-FDi01-25×36 dichroic mirror (Semrock), FF01-483/32-25 and FF01-525/45-25 emission filters (Semrock) was used. Chemiluminescent emission was induced by incubation with 50 μM furimazine. For Mermaid2, a FF01-438/24-25 excitation filter, a FF458-Di02-25×36 dichroic mirror (Semrock) and the image splitting optics with the same setup for LOTUS-V were used. For VSFP BF1.2, a FF01-500/24-25 excitation filter, a FF520-Di02-25×36 dichroic mirror (Semrock) and the image splitting optics equipped with a FF580-FDi01-25×36 dichroic mirror, FF01-542/27-25 and FF01-624/40-25 emission filters (Semrock) were used. For ArclightQ239, a FF02-472/30-25 excitation filter, a FF495-Di03-25×36 dichroic mirror and a FF01-520/35-25 emission filter (Semrock) were used. For FlicR1.0, a FF01-562/40-25 excitation filter, a FF593-Di03-25×36 dichroic mirror and a FF01-624/40-25 emission filter (Semrock) were used. For QuasAr2, a homemade total internal reflection fluorescence (TIRF) microscope based on an IX71 inverted microscope (Olympus) with a 60x, NA 1.40, Plan Apo oil-immersion objective (Olympus), a 638 nm red diode laser (Coherent) and an Evolve512 EMCCD camera (Photometrics) was set up. A Di01-R405/488/561/635-25×36 dichroic mirror and a FF01-692/40-25 emission filter (Semrock) was used for the imaging.

To activate ChR2(H134R) and eNpHR3.0 during imaging, stimulating light from a light emitting diode (LED) source (LightEngine SPECTRA, Lumencor) was irradiated during the processes for image readout and accumulated charge clearing on the camera (dead time) as reported previously (**Fig.15a**) (45, 46). Briefly, a WF1973 multifunction generator (NF Corporation) made the pulsed signals for turning on/off the

stimulation light based on the exposure time-out signals from the camera. The entire illumination period was controlled by LabView (National Instruments) (**Fig.15b**). The power densities of stimulation light for ChR2(H134R) and eNpHR3.0 were 25.5 mW/cm^2 (438 nm) and 47 mW/cm^2 (580/27 nm), respectively. These were carefully adjusted to avoid unintended cross activation following a previous report using same optogenetic actuators (42). To make stimulation light irradiated from above the culture dish, a halogen lamp for the bright field image was replaced with a liquid light guide coupled to a LightEngine SPECTRA (Lumencor).

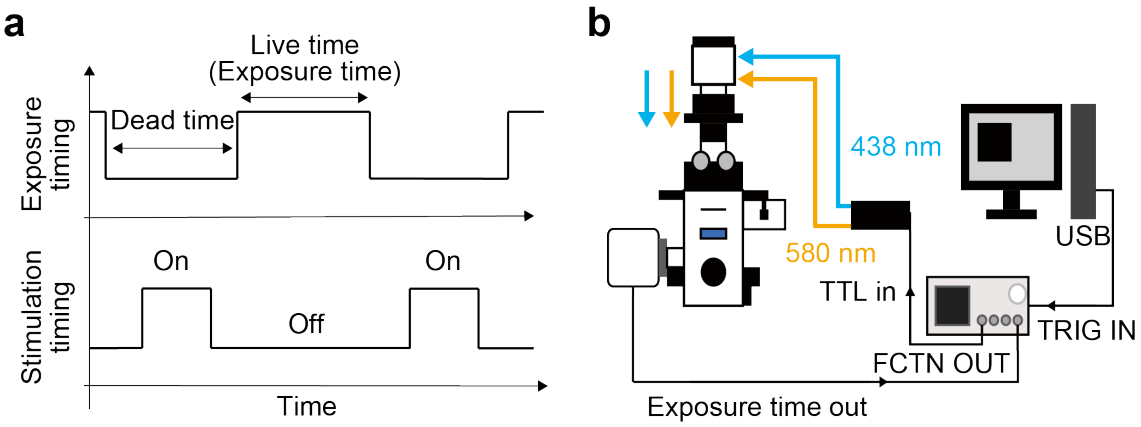

Figure 15 System setup for optogenetic stimulation during dead time (**a**) The stimulation light was irradiated during dead time. (**b**) The system setup to activate ChR2(H134R) and eNpHR3.0. Exposure time-out signals for triggering the multifunctional generator were transferred from a camera thorough 50 Ω BNC cables. Pulse signals generated from a multifunctional generator were transferred to a LightEngine (Lumencore) via transistor-transistor logic (TTL) input to turn the light on/off. A PC was used to record image data and to control the on/off timing of the stimulation light. Arrowheads indicate the signal flow. 438/24 nm and 580/27 nm light were irradiated from above the culture dish. Stimulation was achieved by replacing the halogen lamp with a liquid light guide coupled to the LightEngine. The figure is from reference (17).

To check whether chemiluminescence from LOTUS-V itself does not activate a co-expressed optogenetic actuator, chemiluminescence imaging simultaneously with optogenetic stimulation and patch-clamp experiment was performed. Light stimulation for ChR2(H134R) and eNpHR3.0 (475 nm and 540 nm, respectively) from a mercury arc lamp was irradiated for 1 s to activate them. Imaging and patch clamp experiment were performed as described above except that ORCA-Flash 4.0 digital CMOS camera was used.

4.4. Result and discussion

4.4.1 Activity of an optogenetic actuator during chemiluminescence

Although it seems obvious that optogenetic actuators are not activated if the excitation light is absent during imaging, one might be concerned that the chemiluminescence signal from LOTUS-V could activate them. To explore this possibility, I performed chemiluminescence imaging simultaneously with optogenetic stimulation and patch clamp recording. First, to check the compatibility with ChR2(H134R), LOTUS-V and ChR2(H134R) were expressed in HEK293T cells (**Fig.16a**). During light stimulation by a mercury arc lamp, significant depolarization was confirmed as reported previously (**Fig.16b**) (18), while it did not happen upon addition of furimazine (f.c. 50 μM) (**Fig.16c and f**). Moreover, while light stimulation for eNpHR3.0 also caused significant hyperpolarization, the addition of furimazine (f.c. 50μM) did not evoke hyperpolarization (**Fig.16d,e and g**). These results demonstrated that LOTUS-V chemiluminescence could not activate optogenetic actuators.

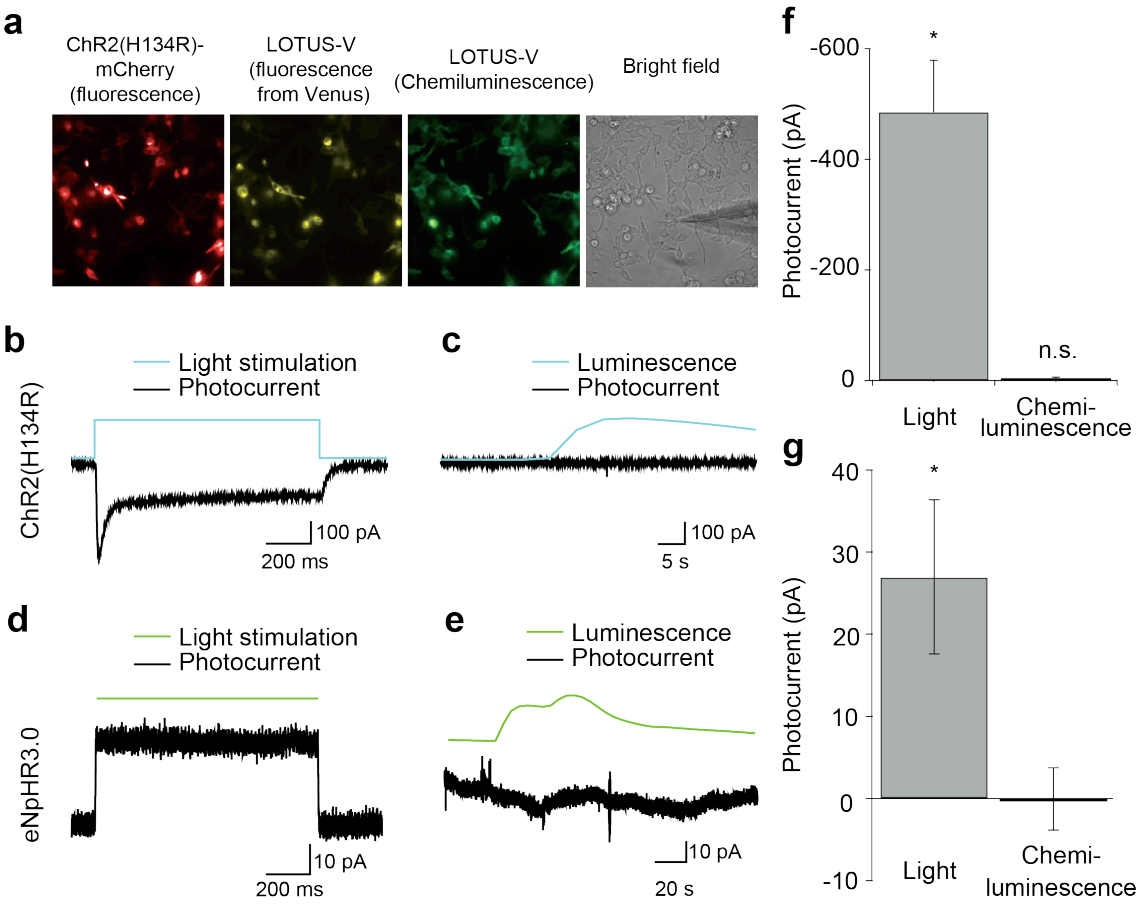

Figure 16 Photocurrent induced by chemiluminescence. (**a**) The example images showing fluorescence, chemiluminescence and bright field to check the expression of ChR2(H134R) and LOTUS-V. (**b-d**) Photocurrent of ChR2(H134R) induced by (**b**) 475 nm light stimulation and (**c**) LOTUS-V chemiluminescence. (**d**) Photocurrent of eNpHR3.0 induced by (**d**) 540 nm light stimulation and (**e**) LOTUS-V chemiluminescence. (**f-g**) Photocurrent of (**f**) ChR2(H134R) and (**g**) eNpHR3.0 induced by light stimulation and LOTUS-V chemiluminescence (n=4 and 5, respectively; $p < 0.05$ for light stimulation in both cases; paired Student's t-test).

4.4.2 Compatibility with optogenetic stimulation

To validate the compatibility of LOTUS-V with multiple optogenetic actuators, voltage imaging in PC12 cells co-expressing LOTUS-V, ChR2(H134R) and eNpHR3.0 was conducted (**Fig.17-18)**. Blue light pulses (438 nm, 25.5 mW/cm^2) rapidly increased LOTUS-V signal, reflecting depolarization of membrane voltage by ChR2(H134R) activation ($\Delta R/R_0$ = 2.9±0.1% [mean ± SE], n=12 sessions). In contrast, orange light pulses (580 nm, 47 mW/cm^2) decreased LOTUS-V signal rapidly ($\Delta R/R_0$=-1.5±0.2% [mean ± SE], n=3 sessions), reflecting hyperpolarization by eNpHR3.0 activation. Importantly, co-irradiation with blue light pulses during orange light pulses increased LOTUS-V signal with an attenuated maximum value compared to that obtained with blue light alone ($\Delta R/R_0$=2.1±0.1% [mean ± SE], n=6 sessions) (**Fig.17**) as described previously (42). In the absence of optogenetic actuators, such signal changes were not observed, and thus these changes reflect voltage changes (**Fig.17 and 18b**). The same experiment was performed using various fluorescent GEVIs for comparison. Although very weak excitation light (for VSFP BF1.2, 500 nm, 1.14 mW/cm^2; for Mermaid2, 438

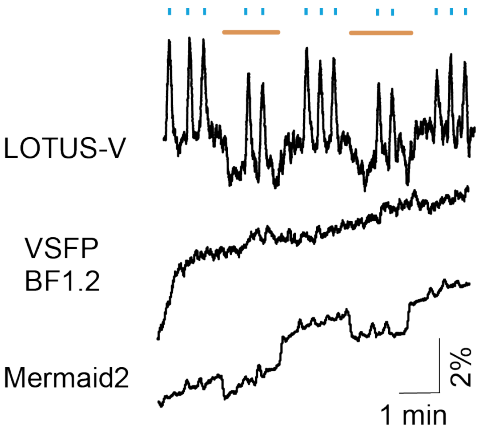

Figure 17 The signals of LOTUS-V, VSFP BF1.2 and Mermaid2 in PC12 cells with optogenetic stimulation (ChR2(H134R) and eNpHR3.0). Blue and orange bars indicate the durations of blue and orange light irradiation, respectively. The $\Delta R/R_0$ processed by the moving average (window length of 50 frames) is shown. The figure is from reference (17).

nm, 2.28 mW/cm^2) was used, rapid upward drift of the baseline was observed (**Fig.17**; +0.72%/min and +0.59%/min for VSFP BF1.2 and Mermaid2, respectively; in contrast, only +0.03%/min for LOTUS-V), which might be caused by differential photobleaching of fluorescent proteins. To quantitatively compare the result, the baseline of the Mermaid2 signal was corrected by single exponential curve fitting (7). During eNpHR3.0 activation, the signal decreased less efficiently ($\Delta R/R_0$=-1.0±0.1% [mean ± SE], n=3 sessions), while during ChR2(134R) activation, no obvious signal change was detected ($\Delta R/R_0$=0.4±0.1% [mean ± SE], n=12 sessions). Considering that Mermaid2 has a larger dynamic range than LOTUS-V (48.5±3.5%/100 mV vs 21.0±0.9%/100 mV), it was a surprise that depolarization caused by ChR2(H134R) activation was hardly observed with Mermaid2. This significant difference between LOTUS-V and Mermaid2 upon blue light irradiation ($p < 0.0001$, n = 12 sessions, Wilcoxon rank sum test) could be caused by constitutive activation of ChR2(H134R) by the excitation light. In contrast, green (ArclightQ239), red (FlicR1.0) and near-infrared (QuasAr2) fluorescent GEVIs, which are known to detect electrophysiologically manipulated hyperpolarization (3, 8, 10), failed to detect hyperpolarization caused by eNpHR3.0 activation, suggesting that the excitation light for these fluorescent GEVIs constitutively activated eNpHR3.0 (**Fig.18c-e**). Interestingly, VSFP BF1.2 was not sensitive enough to detect depolarization, since ArclightQ239 excited by light closer to the wavelength of ChR2(H134R) absorption was able to detect it (Arclight, 472 nm, 1.01 mW/cm^2; VSFP BF1.2, 500 nm, 1.14 mW/cm^2) (**Fig.17 and 18c**). Moreover, blue light pulses increased the signal of QuasAr2 even in the absence of optogenetic actuators, exposing difficulties

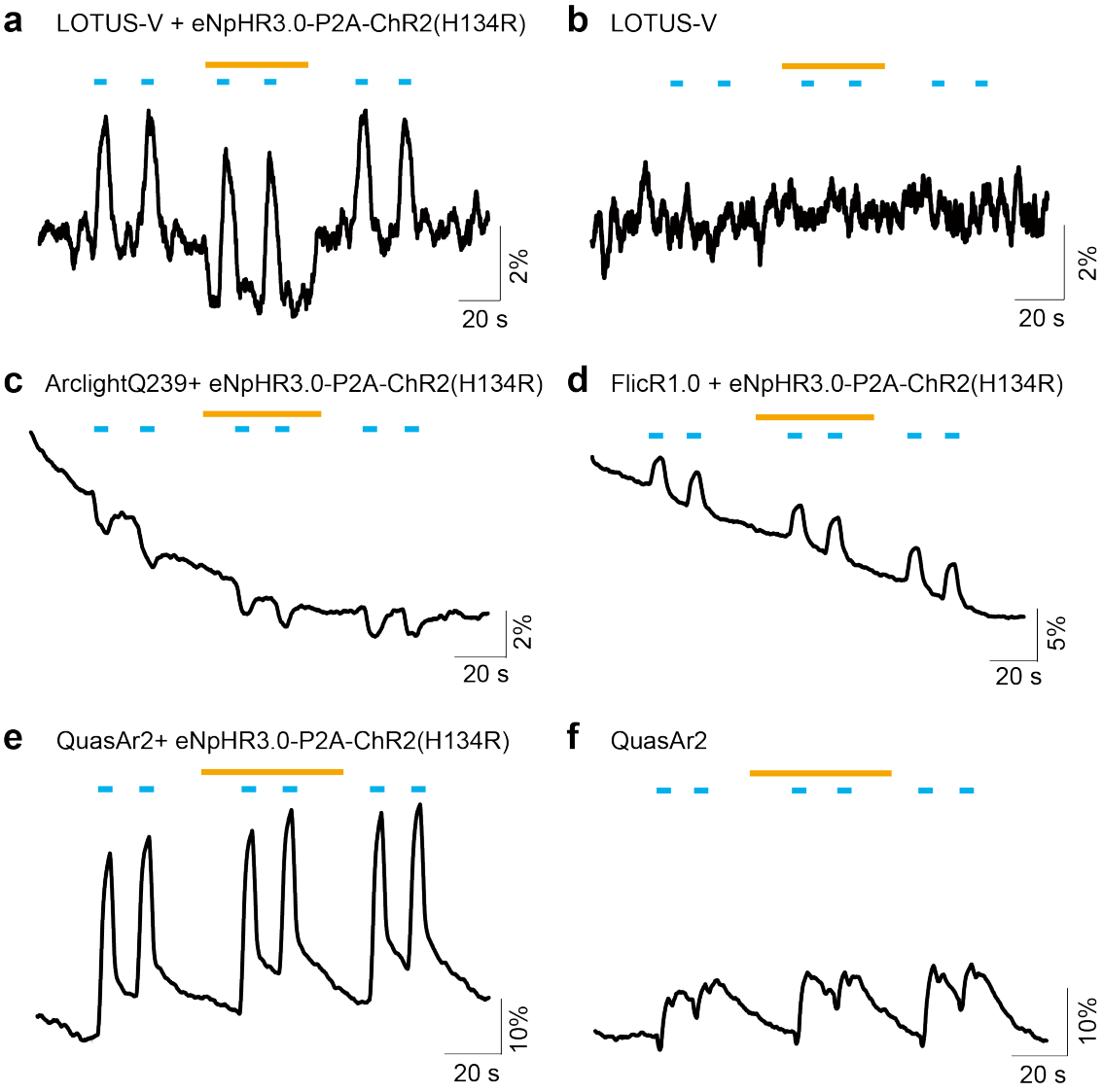

Figure 18 Voltage imaging using various GEVIs with optogenetic stimulation. (**a,b**) The signal of LOTUS-V in the presence (**a**) or absence (**b**) of ChR2(H134R) and eNpHR3.0. (**c,d**) The signal of ArclightQ239 (**c**) and FlicR1.0 (**d**) in PC12 cells. (**e,f**) The signal of QuasAr2 in PC12 in the presence (**e**) or absence (**f**) of ChR2(H134R) and eNpHR3.0. The signals processed by the moving average (window length of 20 frames) is shown. The figure is from reference (17).

in distinguishing a real signal with the "All-optical electrophysiology" previously described (10).

These results clearly show that LOTUS-V offers voltage imaging with

unrestricted optogenetic perturbation, and without upward baseline drift that would be problematic in long-term imaging.

4.5. Perspective

Here, I showed that LOTUS-V is a powerful tool to investigate voltage dynamics in conjunction with optogenetic actuators. Currently, optogenetic manipulation is often used to activate genetically defined subpopulations in specific brain areas rather than in single neurons (49). Therefore, imaging with LOTUS-V is a good partner for optogenetic manipulation because it is better at population imaging, for instance brain activity recording **(**see **Next section)**. Since LOTUS-V is a genetically encoded indicator, "all-optical electrophysiology" with LOTUS-V would be useful to investigate the information processing that is cooperatively achieved by different genetically defined subpopulations in a brain.

Chapter5 NEURAL ACTIVITY RECORDING IN A HEAD-FIXED MOUSE

5.1. Introduction

It is known that electrophysiological field potential dynamics are related to brain function. So far, electrophysiological and fluorescence-based methods have been developed and widely used to detect it. Electroencephalography (EEG) is a popular, clinically relevant, method to detect brain-wide networks, while local field potential (LFP) recording detects more detailed dynamics in localized micro-networks (50). Fluorescence-based techniques, using a voltage sensitive dye is also widely used because of its high-spatiotemporal resolution (51). These are powerful and indispensable techniques for current neuroscience, but are unable to distinguish genetically defined subpopulations. Therefore, a technique that can extract the synchronized activity from genetically defined subpopulations are highly desirable for further elucidation of brain function.

5.2. Purpose and significance

Voltage imaging with GEVIs is a powerful technique to address this issue. Since GEVIs are genetically encoded, one can perform tissue or cell-type-specific imaging at microcircuit level, as well as whole-brain macroscopic imaging (52). Therefore, I investigated whether LOTUS-V can detect the neural activity from an awake head-fixed mouse.

5.3. Materials and methods

Preparation for *in vivo* voltage imaging. C57BL/6JJmsSlc male mice (Japan SLC, Inc.) were housed in the Osaka University Animal Facility and were supplied with food and water *ad libitum*. The AAV vector encoding LOTUS-V was injected into the primary visual cortex (V1) of the mice at postnatal day P35-40 as described previously (53). During surgery, the mice were anesthetized with initially 2% and laterly 1% isoflurane. A small hole (~1 mm diameters) at the skull was made over the left V1 (2.1 mm lateral to the midline, 0.3 mm rostral to lambda at a depth of 300 μm) using a dental drill. 375 nl of AAV crude solution was injected into the left V1 over 15 min period, using a UMP3 microsyringe pump (World Precision Instruments).

3 weeks to 5 months after the virus injection, the mice were anesthetized with 1-1.5 % isoflurane, and the expression of LOTUS-V was confirmed by two-photon imaging. A titanium head plate was attached to the skull using dental cement, and a cranial window with 1.5 mm diameter was made around the virus injection site. 4% low-melting agarose gel dissolved in HEPES-buffered saline (10 mM HEPES, pH 7.3, containing 150 mM NaCl, 2.5 mM KCl, 1 M $MgCl_2$, 1 M $CaCl_2$) covered the brain surface until chemiluminescence imaging started. Venus fluorescence was imaged with a FVMPE-RS two-photon microscope (Olympus), equipped with a Mai Tai DeepSee Ti:sapphire laser (Spectra-Physics) at 920 nm and a 4x dry objective, 0.28 N.A. (Olympus) (or a 25x water immersion objective, 1.05 N.A. (Olympus)) to check expression level and location. Image acquisition was controlled by a FV30S-SW image acquisition and processing software (Olympus).

For chemiluminescence imaging, the primary alcohol solvent of furimazine solution (Promega) was evaporated with a VDR-20G vacuum desiccator (Jeio Tech) and a BSW-50N belt drive rotary vane vacuum pump (Sato Vac Inc.) overnight in the dark. Then, finally the precipitate was dissolved in propylene glycol (up to 5 mM) to minimize the effect on brain function, given by the solvent. This solution was kept at -30°C as stock solution.

Before imaging, an O-ring was attached on the head plate using Kwik-Sil silicon adhesive (World Precision Instruments) (**Fig.19)**. This pool area was used to keep 200 µl of 50 µM furimazine solution, dissolved in HEPES buffered saline, over the cranial window. This O-ring pool was finally covered by a cover glass with the Kwik-Sil adhesive. The surface of the head plate and the dental cement were stained black using Touch Up paint X-1 matte black (SOFT99) to suppress reflected chemiluminescence signals. Also, a black guard spray (Fine Chemical Japan) was used to stain the inside of the mouse cage black.

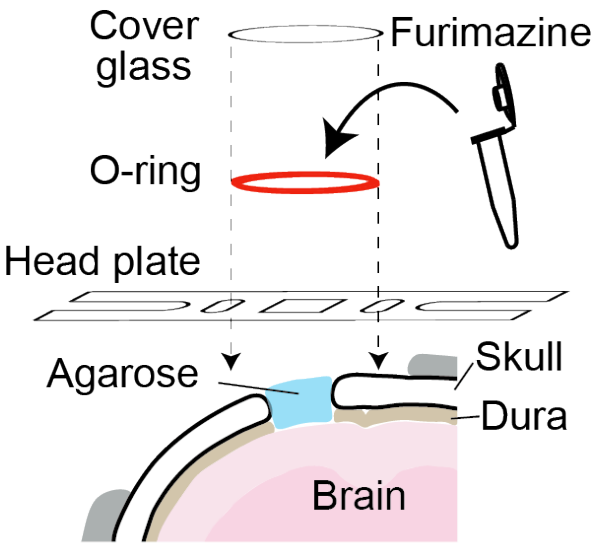

Figure 19 The illustration of the prepared cranial window. The figure is from reference (67).

***In vivo* imaging of head-fixed mice.** A Lumazone *in vivo* luminescence imaging system (Molecular Devices) equipped with an AT-X M100 PRO D macro lens (Tokina), a W-VIEW GEMINI image splitting optics (Hamamatsu Photonics), a C8600-05 GaAsP high-speed-gated image intensifier unit (Hamamatsu Photonics) and an Evolve Delta 512 EMCCD camera (Photometrics) were used. To minimize the contaminated signal from visual stimulation, emission filters (NanoLuc channel; FF02-472/30-25 and FF01-483/32-25, Venus channel; FF01-537/26-25 and FF01-542/27-25) were installed in the image splitting optics. During the recording, the mouse was placed on a custom-made running disk and its head was held with the attached head plate (**Fig.20**). The rotary encoder was attached to the running disk in order to record the running speed under the control of LabView (National Instruments). Camera binning was set at 4.

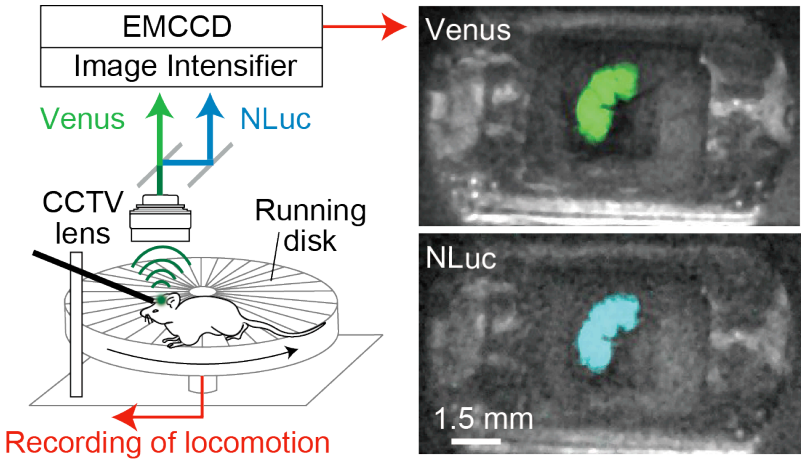

Figure 20 Schematic drawing of head-fix system. Chemiluminescence images in NanoLuc and Venus channels (right). The figure is from reference (67).

For visual stimulation, the blue laser from Sapphire 458 LP (Coherent) was coupled to a 3-mm-diameter liquid light guide (Thorlabs) through a F35 plano-convex lens (Sigma Koki), a chopper wheel (Thorlabs), a F40 plano-convex lens (Sigma Koki), an iris diaphragm (Sigma Koki) and a 12.7-mm-aperture optical shutter (Thorlabs)

(**Fig.21a)**. The tip end of the liquid light guide was covered by a thin white tape to protect the mouse retina. Then, output power density was finally 0.55, 1.10, and 1.65 mW/cm^2 at the surface of the eye. Visual stimulation was performed with these different light intensities for each animal. Light pulse (2 ms duration with 23-ms interval (40 Hz) for a single pulse) was delivered for 1 s with intertrial interval of 7 s (**Fig.21b**). The stimulus trial was repeated 15 times at each light intensity. Imaging was also performed at 40 Hz (exposure time, 20 ms; and dead time, 5 ms) and a single light pulse for visual stimulation was irradiated to the eye only during the dead time (45, 46). Exposure of an EMCCD camera and gate-on timing of an image intensifier unit were

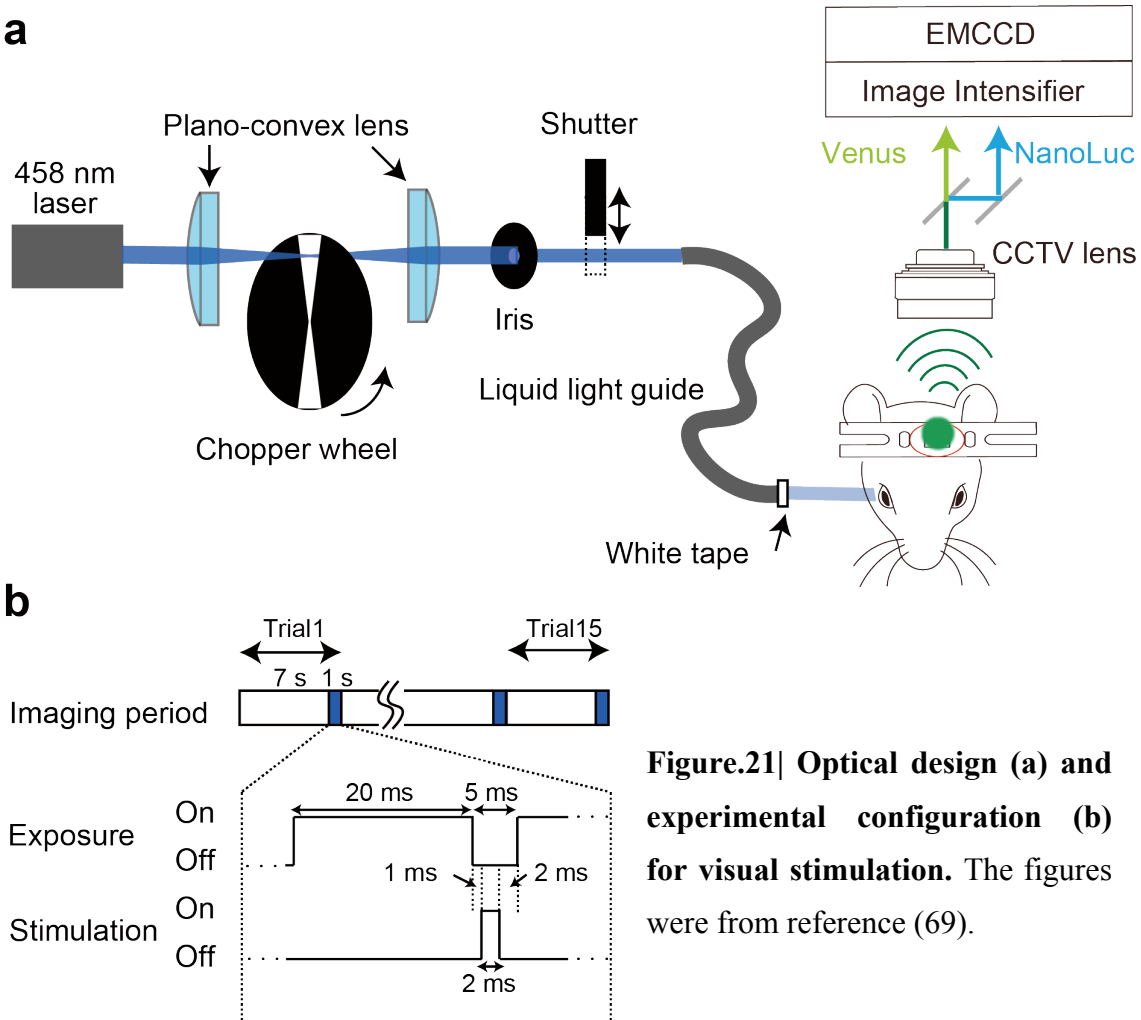

Figure.21| Optical design (a) and experimental configuration (b) for visual stimulation. The figures were from reference (69).

controlled by a TTL signal from a multifunction generator (WF1973, NF Corporation) based on an output signal from an optical chopper system.

Data analysis. All of the imaging data were processed by Fiji and MATLAB (Mathworks).

The "baseline" for the calculation of $\Delta R/R_0$ means the signal when the mouse was immobile (resting state, <5 cm/s, which was set based on the noise fluctuation level of the detected locomotion velocity when mice were actually not moving). As for visual stimulation trials, "baseline" means that a mouse was in resting state during the absence of stimulation. When the movies of head-fixed mice were analyzed, the ROI was created in the same way as *in vitro* experiments, and the data was analyzed similarly.

To statistically compare the results obtained from different animals, $\Delta R/R_0$ in each animal was z-normalized (54) to obtain "z-normalized $\Delta R/R_0$." Z-scored values were calculated by subtracting the average baseline signals in resting state from individual raw values and by further dividing the difference by the baseline standard deviation. For the analysis of visual stimulation, the first 0.5 s data was used as the signal during visual stimulation.

5.4. Results and discussion

5.4.1. Activity in the primary visual cortex upon visual stimulation

To test whether LOTUS-V is useful for brain activity imaging in an awake mouse, a head-fixed imaging system was applied to examine it. With the AAV-mediated expression system, LOTUS-V was locally expressed in V1, and the population of local V1 neurons was labeled (**Fig.22a-c**). It is well known that V1 neurons are the ones strongly responding to the visual input (14, 51, 55), and thus initially, the signal change of LOTUS-V during visual stimulation was investigated (**Fig.22d**). Since light illumination for visual stimulation can be contaminated in the acquired images bacause of the high sensitivity of the detection system (an EMCCD with an image intensifier unit), visual stimulation was only performed during the camera's dead time to avoid such contamination (**Fig.21, see Method section**) (45, 46). Weak light did not show a significant difference compared to baseline (n.s. at 0.55 and 1.10 mW/cm^2, Wicoxon rank sum test). However a light intensity-dependent response in the LOTUS-V signal became apparent at higher power density of incident illumination ($p<0.05$ at 1.65 mW/cm^2, Wicoxon rank sum test) (**Fig.22d**). This result suggested that LOTUS-V can

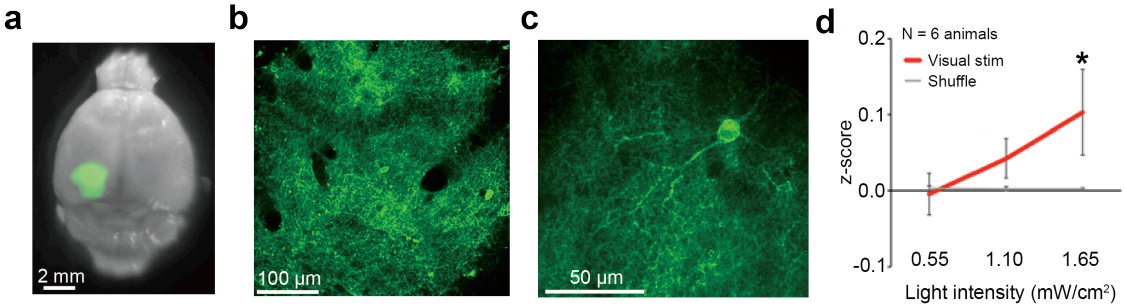

Figure22 V1 neurons expressing LOTUS-V (a-c) and their activity depending on light intensity of visual stimulation (d). The figure is from reference (69).

detect activation of V1 neurons in an awake animal.

5.4.2. Locomotion-dependent activity in the primary visual cortex

Although V1 neurons are popular to study visual stimulation, it is also well known that neural activity in V1 is mildly correlated with locomotion of mice even without visual input (56–58). Therefore, to examine application to other inputs, I investigated whether the LOTUS-V signal could detect such locomotion-dependent increases of neural activity.

The speed of spontaneous locomotion of the head-fixed mouse was measured by the rotation of a running disk, and simultaneously the LOTUS-V signal from V1 neurons was recorded (**Fig.20 and 23**). The LOTUS-V signal significantly increased (**Fig.23a**; for all sample, $p<0.0001$, n=707871 and 31653 time-points for resting and active states, respectively, Wilcoxon rank sum test, **Fig23b**; for averaged values from each mouse, $p<0.05$, N=7 animals, Wilcoxon signed-rank test) while mice were moving

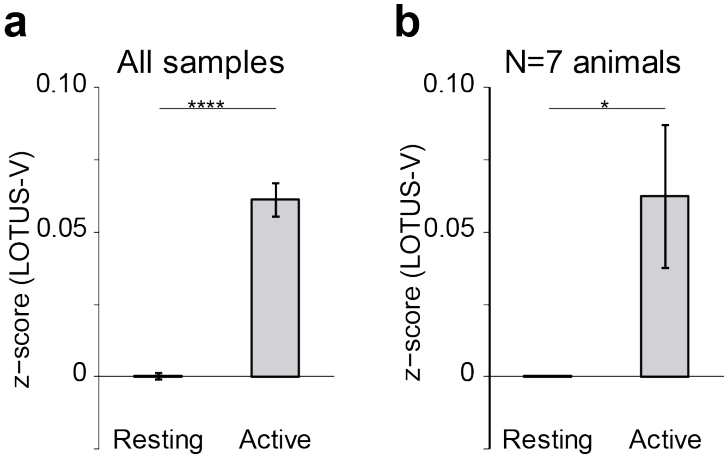

Figure 23 Bar plots of z-normalized $\Delta R/R_0$ in resting (<5 cm/s) and active (>5 cm/s) states of head-fixed mouse, using (a) all time-points, or (b) average values from each mouse. The figure is from reference (67).

on the running disk, confirming its usefulness to monitor local brain activity irrespective of the input modalities.

5.5. Perspective

In this chapter, I confirmed that LOTUS-V can detect the activity of V1 neurons of an awake mouse independently of variable sensory modalities. As I showed in the chapter3, the SBR of voltage imaging with LOTUS-V is superior to that of fluorescent voltage indicators owing to the absence of autofluorescence from tissue samples. Therefore, LOTUS-V must also be useful to detect neural activity in deep brain regions without using a prism or an optical fiber that potentially disturbs normal brain activity or circuitry. Also with a genetically encoded tool, we can perform tissue or cell-type-specific imaging, as well as whole-brain macroscopic imaging with the use of LOTUS-V, all of which are widely required in neuroscience research (52).

Chapter6 NEURAL ACTIVITY RECORDING IN FREELY INTERACTING MICE

6.1. Introduction

To detect brain activity during more complicated behavioral tasks, both electrophysiological and fluorescence-based techniques have been optimized for the recording from a freely moving animal (19, 59–62). Nonetheless, several technical limitations still exist in those methods. One limitation is the requirement of special knowledge and complicated instrumentation for electrophysiology or optics. Another limitation is that the head of a freely moving animal must be connected to a fiber to provide light or electricity. These limitations restrict the applicability to freely moving subjects, especially in the setting of multiple animals spontaneously interacting when the fibers tangle. Therefore, the development of a fiber-free detection system, which allows investigation of neural networks regulating social behaviors and related psychiatric diseases, is strongly required to further elucidate brain function.

6.2. Purpose and significance

To wirelessly detect brain activity from freely behaving animals, I propose a fiber-free imaging system with LOTUS-V. For example, when we take movies of chemiluminescence emitted by fireflies at night, we just use a digital camera (or even a smart phone). Therefore, I expected that LOTUS-V could be useful for simple brain activity recording, and thus for the investigation of socially evoked brain activity.

6.3. Materials and methods

Gene construction and AAV preparation for LOTUS-V (D129R). The construction of pAAV2-hSyn-LOTUS-V(D129R) and preparation of AAV encoding LOTUS-V(D129R) were performed as before.

***In vivo* imaging of freely moving mice.** The same equipment was used for imaging a head-fixed mouse, except that no emission filters, a C8600-05 GaAsP image intensifier unit (Hamamatsu Photonics) and a HF12.5SA-1 wide-angle lens (Fujinon) were used (**Fig.24**). The camera binning was set at 8 and 2 for single mouse and multiple mice recording, respectively. The frame rate was set at 10-100 Hz depending on the signal intensity from the specimens.

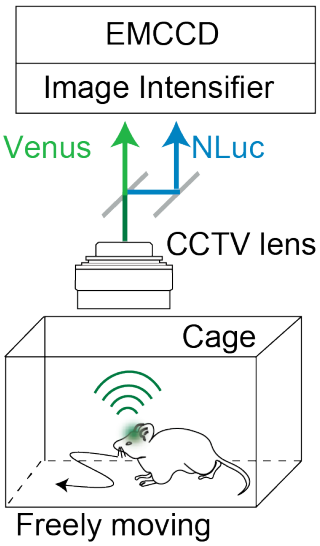

Figure 24 Schematic drawing of imaging of a freely moving mouse. The figure is from reference (67).

Overlay images were made to demonstrate that the signals were correctly coming from the cranial window, or to capture the shapes of mice clearly for interaction analysis (**Fig.26a and 27a**). The chemiluminescence images in the dark and the

bright-field images under 632 nm LED (LightEngine SPECTRA, Lumencor) illumination were captured alternately every 50 ms as previously described (46, 63). The timing of LED illumination was controlled by a TTL signal from a multifunction generator (WF1973, NF Corporation), which was generated based on an output signal from the exposure time-out signals from a camera. The LED light was illuminated for 5 ms from the initiation of the camera exposure on alternate frames.

Data analysis. Before the analysis, the "background image", obtained by averaging 1000 blank images taken with the closed shutter of a camera, was subtracted from the acquired images. The signal intensity after background subtraction was sometimes lower than 0 due to the fluctuation of background noise, which is also often observed in single molecule analysis (64). This negative value was almost 0, however it can disperse the distribution of ratio values. Therefore, the absolute value of this minimum value was added to the all values in both NanoLuc and Venus channels. If the value in the NanoLuc channel became 0, the frame at that time point was removed before the data analysis. The "baseline" for locomotion analysis means that animals were in resting state (<1 cm/s, which was set by referring to the previous study (57)), while the one for interaction analysis means that an animal was distant enough from others (distant state, >4 cm) or in a “distant and resting” state.

For the imaging of single freely moving mice, the chemiluminescence spot in the field of view was automatically tracked by means of “Particle Track Analysis” (PTA ver1.2), while for imaging of multiple mice, the cranial window in the head plate was

manually tracked with “Manual Tracking” (ImageJ plugin). For automatic tracking, chemiluminescence images were processed by Gaussian blur filter with radius value set to 1.0. Each movie was separated into NanoLuc and Venus channels, referring to the bright field image. To accurately detect the chemiluminescent spot, the reference movie containing the intensity information of both channels was created from these separated movies by the “AND” function of ImageJ. Since the signal intensity largely changed depending on the angle of the mouse head, some of the frames were difficult to track automatically. Therefore, when the signal was not automatically detected over 3 frames by PTA, these missed frames were excluded from the data. If the signal appeared within 3 frames from when the last signal was detected, PTA recognized them as a series and continued automatic tracking. Linear interpolation was performed to fill such missing values at most 2 frames.

Shot noise was the main source of artifact in the acquired image. Shot noise is a variation in the observed signal due to two factors, firstly statistical fluctuation the low number of the photons emitted from a luminescent specimen, and secondly the corresponding electrons generated in response to the emitted photon. Such background noise often overlapped with the actual signal in the image, hampering automated signal detection, and skewing ratiometric intensity assessments. Therefore to combat this phenomenon, stringent ratio values ranging from 0.8 to 2.0, based on the results in head-fixed mice (the averaged ratio value plus or minus threefold the value of standard deviation, N=8 animals), were used for the data analysis. Locomotion speed was estimated from the frame-by-frame position change of the center of the

chemiluminescence spot. The trajectories shown in **Fig.26a and 27a** were drawn with pseudo color, which was based on z-normalized $\Delta R/R_0$ or the length of the line segments.

The SBR was calculated before background subtraction by dividing the averaged signal intensity of NanoLuc and Venus channels by the background intensity from non-specimen area. When the SBR was lower than 0.12, due to substrate consumption, automatic tracking couldn't properly distinguish the signal from shot noise. Thus, data with SBR lower than 0.12 were excluded from the analysis. The total imaging time period for each mouse was calculated by measuring the duration from initiation time to the time when SBR reach to 0.12 or higher.

During imaging of multiple mice, one out of the four mice didn't spontaneously interact with others throughout the experiment probably because of surgical damage (**Fig.27a**). To quantitatively assess how immobile this mouse was, the fraction of the active state (>1 cm/s) (57) was calculated in each mouse. The average fraction of the other mice used for the experiments was 64.2±7.8% [mean ± SE.] (N=11 animals), while that of immobile one (N=1) was only 2.1%. "Chi-squared test for outliers", following justification of normal distribution (Kolmogorov–Smirnov test, $p>0.05$, N=12 animals), systematically detected this quiet animal as an outlier ($p<0.05$), and thus the data of this mouse was excluded from the analysis.

For interaction analysis, the area of each mouse in a 2D image was approximated by three variable circles (**Fig.25**) in reference to the previous study (65). Using the "Manual Tracking" ImageJ plug-in, the positions of a nose (x_1, y_1), head plate

(x_2, y_2) and tail root (x_3, y_3) were tracked to obtain their coordinate information. This information was used to define the positions of a dorsum (($x_3 + 2x_2 – x_1$)/2, ($y_3 + 2y_2 – y_1$)/2) and a cervix ($2x_2 - x_1$, $2y_2 - y_1$). Then, the centers of three variable circles were located at the head plate, the cervix and the dorsum, for Circle1, 2 and 3, respectively. For Circle1 and 2, the radius of each circle was set as the distance between the head plate and the nose, while for Circle3, set as the distance between the dorsum and the tail root (**Fig.25a**). After the approximated area of each mouse was defined, the distances between the nose of the target mouse and the edge of each circle were calculated. Then, finally the shortest one was used for the index of the interaction analysis (**Fig.25b**). The distance was represented as a negative value when the nose was the inside of the circle.

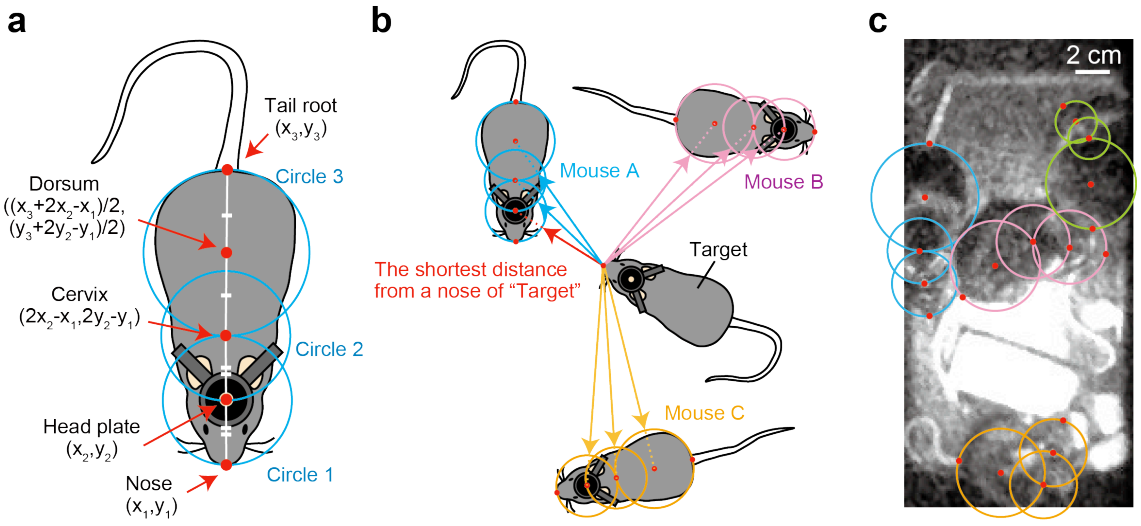

Figure 25 Measurement of the distance between interactively locomoting mice. (**a-b**) Image illustrating the definition of the approximate areas of the mouse (**a**) and distance between the target mouse and other mice (**b**). (**c**) An example of an overlay image of the bright field and approximate mouse areas. The color of each circle indicates the different individual mice. The figure is from reference (67).

6.4. Results and discussion

6.4.1. Measurement in a freely moving mouse

To confirm whether voltage imaging with LOTUS-V can be conducted at fiber-free, chemiluminescence signal from V1 neurons of a freely moving mouse was captured in a dark box. Importantly, in contrast to the fiber-coupled system, the optics were completely detached from the mouse (**Fig.24**). When the imaging was performed, intense chemiluminescence signal from the targeted brain region was continuously observed for at most 7 h (3.10±0.45 h [mean ± SE], N=16 mice). Since TEMPO (19), which is a recently reported fiber-coupling method, can be performed for ~1 h, a fiber-free method based on LOTUS-V is superior for long-term imaging. This suggests that although chemiluminescent imaging with LOTUS V is limited by substrate consumption, this effect is milder than the photobleaching seen in fluorescence imaging in vivo.

While the mouse spontaneously moved, the position of the chemiluminescence spot also followed its movement (**Fig.26a**). Then, by using a particle track analysis program, the LOTUS-V signal arising from V1 together with locomotion velocity was automatically detected. As confirmed in the head-fixed system, the LOTUS-V signal increased significantly during the active state (>1 cm/s) of a freely moving mouse (**Fig.26b**; $p<0.0001$, Wilcoxon rank sum test). Next, the results of LOTUS-V expressing animals (N=5 animals) was compared with those of animals expressing voltage-insensitive LOTUS-V(D129R) (N=3) to confirm whether the LOTUS-V signal correctly reflected a real voltage change or were just artifacts of head angle. The

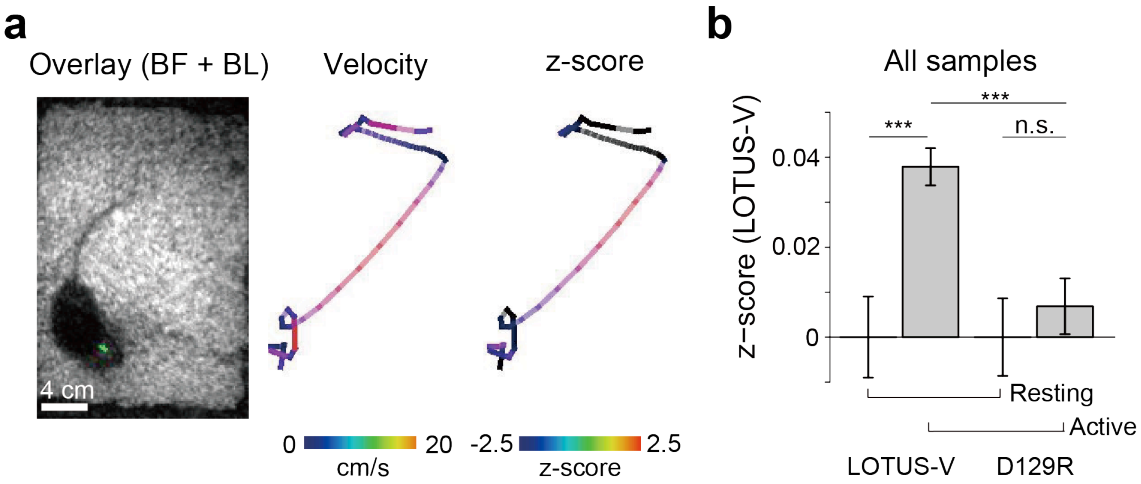

Figure 26 Imaging of a freely moving mouse. (**a**; left) Overlay image of bright field and LOTUS-V chemiluminescence (green). (**a**; middle and right) Pseudo-colored trajectories of locomotion velocity (middle) and z-normalized $\Delta R/R_0$ (right). (**b**) Bar plot of z-normalized $\Delta R/R_0$ in the resting (<1 cm/s) and active (>1 cm/s) states of freely moving mice ($p<0.0001$ for one-way ANOVA with all four categories; resting and active states of LOTUS-V, n=12277 and 57079 time-points from N=5 animals; resting and active states of LOTUS-V(D129R), n=13467 and 26573 from N=3; p-values shown in the panel were calculated using a post-hoc Tukey-Kramer test). The figure is from reference (67).

LOTUS-V(D129R) signals did not change significantly during locomotion (n.s., post-hoc Turkey-Kramer test), and LOTUS-V signal during the active state was statistically higher than LOTUS-V(D129R) signal during the active state ($p<0.001$, post-hoc Turkey-Kramer test). These results certify that the fiber-free method with LOTUS-V can detect neural activity in a freely moving mouse for extended periods of time (~ 7 h).

6.4.2. Measurement in freely moving multiple mice

Since the fiber-free system worked well, next I applied it to multiple mice freely interacting with each other (**Fig.27**). For tracking analysis, the bright-field and chemiluminescence images were taken alternately (46, 63) by illuminating the field of view with a LED every other frame. The target area of each mouse was manually tracked, and locomotion and LOTUS-V signal were measured. As a result, locomotion-driven signal change in V1 of freely interacting mice was successfully detected ($p<0.0001$ for Mouse 1; $p<0.05$ for Mouse2; $p<0.001$ for Mouse 3; $p<0.0001$ for all time points, Wilcoxon rank sum test) (**Fig.27b**), except for the mouse that was quiet throughout the imaging and thus excluded from analysis (see **Methods section**). To my knowledge, this is the first report of simultaneous recording of brain activity from "three" animals freely locomoting.

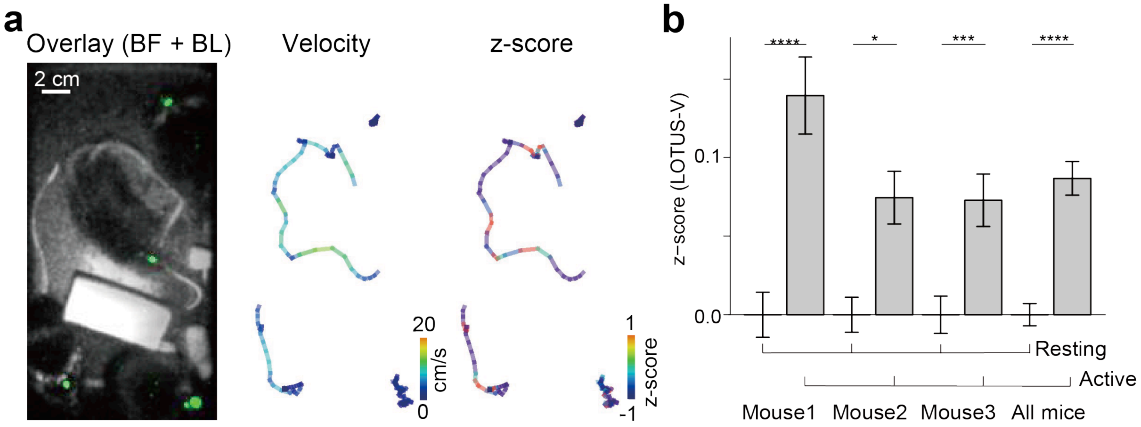

Figure 27 Imaging of a freely moving multiple mice. (**a**; left) Overlay image of bright field and LOTUS-V chemiluminescence (green). (**a**; middle and right) Pseudo-colored trajectories of locomotion velocity (middle) and z-normalized $\Delta R/R_0$ (right). (**b**) Bar plots of z-normalized $\Delta R/R_0$ during resting (<1 cm/s) and active (>1 cm/s) states (Mouse1, n= 4862 and 1935 time-points; Mouse2, n= 8051 and 4099; Mouse3, n= 7062 and 3741; All mice, n= 19975 and 9775). P-values were obtained by a Wilcoxon rank sum test. The figure is from reference (67).

6.4.3. Analysis of interaction-dependent activity

Next, I investigated whether spontaneous interaction activates the V1 neurons (**Fig.28**). For systematic analysis based on the distance between mice, each mouse in the 2D image was approximated by three variable circles (**Fig.25**, see **Method section**) (65). Interestingly, when each mouse approached the others, the activity in V1 increased

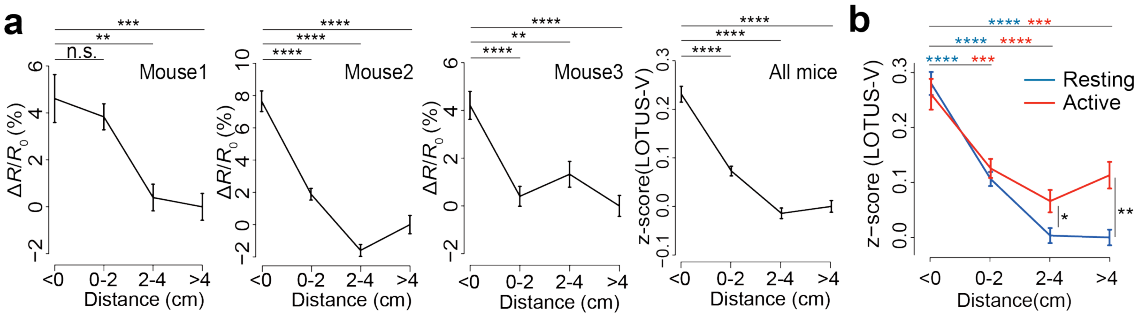

Figure 28 Analysis of interactive freely moving mice. (**a**) Distance-dependent activity of V1 neurons. Plots represent $\Delta R/R_0$ (Mouse1-3) or z-normalized $\Delta R/R_0$ ("All mice") of each distance category (distance from Mouse1, n=665, 2215, 1905, and 2012 time-points for <0, 0–2, 2–4 and >4 cm, respectively; Mouse2, n=1892, 4745, 3747, and 1776; Mouse3, n=2163, 3462, 2048, and 3139). The distant state (>4 cm) was used as a baseline (R_0) to calculate the $\Delta R/R_0$ and for the z-normalization. P-values were obtained by a post-hoc Tukey-Kramer test. (**b**) Distance-dependent activity of V1 neurons in resting (<1 cm/s, blue) and active states (>1 cm/s, red). Data from all mice was used (resting state, n= 3075, 6769, 5214, and 4914 time-points for <0, 0–2, 2–4, and >4 cm, respectively; active state, n= 1645, 3653, 2486, and 2008). The $\Delta R/R_0$ in the "distant and resting" state was used as the baseline for z-normalization. P-values obtained by a one-way ANOVA with all four categories; p <0.0001 in both states. P-values obtained by post-hoc Tukey-Kramer test are shown as blue (resting states) or red (active) symbols, while those obtained by Wilcoxon rank sum test (to compare resting vs active states) are shown in black. Error bars indicate mean ± SE; n.s., not significant; *, p <0.05; **, p <0.01; ***, p <0.001; ****, p <0.0001. The figure is from reference (67).

(**Fig.28a**). Then, the distance- and locomotion-dependent effects were separately analyzed (**Fig.28b**). As a result, I found that locomotion did not significantly increase V1 activity when the distance was small (<2 cm). This result suggested that the interaction with other mice has a competitive impact in V1 compared with the simple exploratory locomotion.

For this result, one might be concerned that chemiluminescence from other mice could work as visual stimulation because V1 neurons are known to respond to visual input. To exclude this possibility, I estimated the power density of LOTUS-V chemiluminescence from the V1 surface.

The number of photons P detected by a camera sensor was calculated from the total analogue-to-digital converter (ADC) counts I as given by;

$$P = \frac{IA_{\mathrm{d}}}{Qt_{\mathrm{ex}}G},$$

where Q is the quantum efficiency of a camera; t_{ex} is the exposure time; G is the radiant emittance gain of an image intensifier unit; and A_{d} is the analog-to-digital conversion factor of a camera. Because the ray divergence θ from the chemiluminescent object was small enough, the fraction of the detected photons F was calculated as;

$$F = \frac{\pi(W_{\mathrm{d}} \tan\theta)^2}{2\pi {W_{\mathrm{d}}}^2},$$

where W_{d} is the working distance of a lens. Therefore, chemiluminescence intensity L, radially emitted from the V1 region was calculated by;

$$L = \frac{hcP}{\lambda F},$$

where λ is the wavelength; h is the Planck constant; and c is the speed of light. As a result, the power density of LOTUS-V chemiluminescence from V1 region was estimated as $(7.6\pm1.0)\times10^{-9}$ and $(9.0\pm1.3)\times10^{-9}$ mW/cm^2 (N=6 animals) at 480 nm and 540 nm, respectively. Since these power densities were lower than the weakest visual stimulation (0.55 mW/cm^2) (**Fig.22d**), the chemiluminescence signal from other mice appears unlikely to influence the result of locomotion and interaction analysis (**Fig.28**).

6.5. Perspective

Collectively, the fiber-free imaging system based on LOTUS-V is a powerful method to monitor neural activity from a target brain area of interactively locomoting mice. As far as I know, this result is the first report that brain activity was recorded simultaneously from "three" freely behaving mice. More importantly, with this fiber-free system, LOTUS-V successfully reported a novel type of V1 activation during the interaction. I expect that when a wireless device for optogenetic manipulation is combined to our system, it may further allow us to wirelessly detect and manipulate neural activity in freely behaving animals (66). Thus, the detailed mechanism of locomotion and distance-dependent activation of V1 region could be investigated. Taken together, LOTUS-V allows us for simple and fiber-free imaging method for freely behaving animals for extended period of time, and thus opens a door to the investigation of neural network regulating social or group behavior of animals.

Conclusion

Here, I show the summary of the achievements of this study;

- The world-first chemiluminescent voltage indicator, LOTUS-V has been developed by a simple and versatile screening method.
- The electrophysiological character of LOTUS-V was confirmed in HEK293T cells, *Xenopus* oocytes and primary culture of hippocampal neurons, and which was good enough to detect a single action potential.
- LOTUS-V detects the drug-induced change in electrophysiological states of hiPSC-CMs, based on the frequency and morphology of action potentials.
- LOTUS-V successfully mitigates motion artifacts by ratiometry, shows superior SBR in thick sample, and thus enables robust and sensitive recording of membrane voltage in moving samples.
- The voltage imaging with LOTUS-V is fully compatible with multiple optogenetic stimulation using e.g. ChR2(H134R) and eNpHR3.0.
- LOTUS-V detects the activity of V1 neurons upon visual stimulation.
- The fiber-free method in conjunction with LOTUS-V detected the locomotion-dependent activity of V1 neurons simultaneously from "three" freely behaving mice.
- Furthermore, this fiber-free method detected the novel type of V1 activation associated with self-locomotive state and interaction with other mice, suggesting that it could be a powerful technique to investigate socially related brain activity of interactively locomoting animals.

Name of Primer	Sequence (5' to 3')
F-*Hind*Ⅲ-VSD_1	AGTCAAGCTTGCCACCATGGAGGGATTC
F-*Eco*R Ⅰ-VSD_1	GCAGAATTCGCCACCATGGAGGGATTC
F-*Bgl*Ⅱ-VSD_1	GACTAGTCTGCCACCATGGAGGGATTC
F-*Eco*R Ⅰ-GVG-VSD_70	GCAGAATTCGGCGTGGGCGAGGAACGAATAGATATACC
F-*Eco*R Ⅰ-GVG-VSD_85	GCAGAATTCGGCGTGGGCGAGAATGAACATGGAG
F-*Eco*R Ⅰ-GVG-VSD_104	GCAGAATTCGGCGTGGGCCGCGTCCAGTTTCGTGTCC
R-VSD_69-*BamH* Ⅰ	ATTGGATCCTGTCTTGTCTCTGG
R-VSD_84-*BamH* Ⅰ	ATTGGATCCCCCCACCATAGACCTG
R-VSD_103-*BamH* Ⅰ	ATTGGATCCCCTACACCAGTAGTAG
R-VSD_239-*Xho* Ⅰ	CATCTCGAGTTGTTGATGGGAATAAAATATTC
R-VSD_243-*Xho* Ⅰ	CATCTCGAGTGAAGCCTTCATTTGTTGATG
R-VSD_249-*Xho* Ⅰ	CATCTCGAGTGATATTGTTCTTCTGCTTGAAGCC
F-*Bam*H Ⅰ-NLuc_1	ATTGGATCCGATGGTCTTCACACTCG
F-*Xho* Ⅰ-NLuc_1	CATCTCGAGATGGTCTTCACACTCGAAG
R-Nluc_171-*Eco*R Ⅰ	GCAGAATTCCGCCAGAATGCGTTCG
R-NLuc_171-x-*Not* Ⅰ	ATTGCGGCCGCTTACGCCAGAATGCGTTCG
F-*Xho* Ⅰ-gfp_1	TATCTCGAGATGGTGAGCAAGGGCGAGG
F-*Bam*H Ⅰ-gfp_1	TTGGATCCGATGGTGAGCAAGGGCGAGGAG
F-*Xho* Ⅰ-gfp_50	TAATCTCGAGATGACCGGCAAGCTGCCC
F-*Xho* Ⅰ-gfp_157	TAATCTCGAGATGCAGAAGAACGGCATCAA
F-*Xho* Ⅰ-gfp_173	TAATCTCGAGATGGACGGCGGCGTGCAG
F-*Xho* Ⅰ-gfp_195	TAATCTCGAGATGCTGCCCGACAACCACTA
F-*Xho* Ⅰ-gfp_229	TAATCTCGAGATGATCACTCTCGGCATGG
R-Venus_49-x-*Not* Ⅰ	ATTGCGGCCGCTTAGGTGCAGATCAGCTTCAGGG
R-Venus_156-x-*Not* Ⅰ	ATTGCGGCCGCTTACTTGTCGGCGGTGATATAGA
R-Venus_172-x-*Not* Ⅰ	ATTGCGGCCGCTTACTCGATGTTGTGGCGGATCT
R-Venus_194-x-*Not* Ⅰ	ATTGCGGCCGCTTACAGCACGGGGCCGTCGCCGA
R-Venus_228-x-*Not* Ⅰ	ATTGCGGCCGCTTACCCGGCGGCGGTCACGAACT
R-gfp_239-x-*Not* Ⅰ	ATTGCGGCCGCTTACTTGTACAGCTCGTCCATG
R-gfp_238-x-*Hind*Ⅲ	AGTCAAGCTTTTACTTGTACAGCTCGTCC
R-gfp_238-x-*Xba* Ⅰ	AGTCTCTAGATTACTTGTACAGCTCGTC
R-gfp_239-*Eco*R Ⅰ	GCAGAATTCCTTGTACAGCTCGTCCATGCC
F-LOTUS-V_D129R	GTCTTCCTAATTTTCTTGCGCATCATCCTCATGATC
F-*Eco*R Ⅰ-P2A-1	AATTCGGAAGCGGAGCTACTAACTTCAGCCTGCTGAAGCAGG
F-P2A-*Not* Ⅰ-22	CTGGAGACGTGGAGGAGAACCCTGGACCTTGC
R-P2A-*Not* Ⅰ	CTCCAGCCTGCTTCAGCAGGCTGAAGTTAGTAGCTCCGCTTCCG
R-*Eco*R Ⅰ-P2A-22	GGCCGCAAGGTCCAGGGTTCTCCTCCACGT
F-*Hind*Ⅲ-eNpHR_1	AGTCAAGCTTGCCACCATGACAGAGAC
R-ERex_7-*Eco*R Ⅰ	GCAGAATTCCACCTCGTTCTCGTAGCAGAAC
F-*Not* Ⅰ-ChR2_1	ATTGCGGCCGCATGGACTATGGCGGCG
R-ChR2_309-x-*Xba* Ⅰ	AGTCTCTAGATTATGGCACGGCTCCGGCCT
F-*Bgl*Ⅱ-VSD_1 kozak	GACTAGATCTGCCACCATGGAGGGATTC

R-gfp_238-x-*Xho* I	CATCTCGAGTTACTTGTACAGCTCGTCC
F-VSD_1 In Fusion	TGTCGTGAACACGCTGGATCCGCCACCATGGAGGG
R-gfp_238 In Fusion	GACGCGGCCCACGCCGAATTCCTTGTACAGCTCGTC
F-gfp_1 In Fusion	GGCGTGGGCCGCGTCCAGTTTCGTGTCCGA
R-gfp238-x In Fusion	CGATAAGCTTGATCCCTCGAGTTACTTGTACAGCTC
F-LOTUS-V_428 *Xho* I del	GAAGAACAATATCACTGGAGATGGTGAGCAAGGG
F-LOTUS-V_277 *Eco*R I del	GCATTCTGGCGGAGTTCGGCGTGGGCC

Table1. The primer list for construction.

Acknowledgements

I would first like to appreciate my thesis advisor Prof. Takeharu Nagai (ISIR, Osaka University). He always supported me and gave valuable advice whenever I was in trouble regarding not only scientific research but also my daily life.

I would also like to acknowledge Prof. Yasushi Okamura (Graduate School of Medicine, Osaka University), Prof. Takeshi Yagi (FBS, Osaka University) and Prof. Masahiro Ueda (FBS, Osaka University) as the second reader of this thesis. I am gratefully indebted to them for their valuable comments on this thesis.

I would also like to appreciate the experts involved in this research project; Dr. Tomoki Matsuda (ISIR, Osaka University) contributed to the development of LOTUS-V; Dr. Kazushi Suzuki (ISIR, Osaka University) contributed to the evaluation of cytotoxicity of furimazine; Ms. Yuka Jinno (Graduate School of Medicine, Osaka University), Dr. Hidekazu Tsutsui (Department of Material Science, JAIST) and Prof. Yasushi Okamura (Graduate School of Medicine, Osaka University) contributed to the electrophysiological characterization in HEK293T cells and *Xenopus* oocytes; Dr. Shinya Ohara and Prof. Toshio Iijima (Graduate School of Life Sciences, Tohoku University) contributed to the electrophysiological characterization in primary culture of hippocampal neurons; Dr. Guirong Bai (ISIR, Osaka University) and Dr. Matthew J. Daniels (Division of Cardiovascular Medicine, Oxford University) contributed to the study in hiPSC-CMs; Dr. Ken Berglund (Department of Neurosurgery, Emory University) contributed to the investigation of the activity of optogenetic actuators during simultaneous chemiluminescence imaging and patch-clamp recording; Dr.

Yoshiyuki Arai and Dr. Tetsuichi Wazawa (ISIR, Osaka University) contributed the microscope setup and data analysis; Dr. Masakazu Agetsuma (ISIR, Osaka University) contributed *in vivo* imaging. Without their contribution, this research project could not be successfully conducted.

I also thank the following contributors; Prof. Thomas Knöphel (Department of Medicine, Imperial college of London) provided me with pCAG-VSFP BF1.2; Prof. Robert E. Campbell (Department of Chemistry, University of Alberta,) provided me with pcDNA3-FlicR1.0 and pAAV2-hSyn-FlicR1.0; Dr. Hiroshi Hama (RIKEN, BSI) instructed me how to prepare primary culture of hippocampal neurons; Dr. Akihiro Yamanaka (Nagoya University, RIEM) provided me with an AAV purification method; Dr. Mitsuhiro Iwaki (RIKEN QBiC) lent me a C8600-05 GaAsP image intensifier unit; the Bionanophotonics Consortium (BNPC) supported my experiments using microscopy.

I would also like to appreciate Humanware Innovation Program ("Program for Leading Graduate Schools" of the Ministry of Education, Culture, Sports, Science and Technology, Japan) and Research Fellowships for Young Scientists (Japan Society for the Promotion of Science). They financially supported me to focus on my doctoral program and research.

Animal experiment. All experimental procedures were carried out in accordance with the Institutional Guidance on Animal Experimentation and with permission from the Animal Experiment Committee of Osaka University (authorization number: 3348).

Statistical Analysis. Statistical analysis was carried out with R software or MATLAB. The type of the statistical analysis was mentioned in the manuscript. All p-values less than 0.0001 were described as “$p<0.0001$.” All statistical tests, except for "Chi-squared test for outliers", were performed as two-tailed test. Statistical significance was set at $p<0.05$.

Reference

1. Inagaki S, Nagai T (2016) Current progress in genetically encoded voltage indicators for neural activity recording. *Curr Opin Chem Biol* 33:95–100.
2. Dimitrov D, et al. (2007) Engineering and Characterization of an Enhanced Fluorescent Protein Voltage Sensor. *PLoS One* 2(5):e440.
3. Jin L, et al. (2012) Single Action Potentials and Subthreshold Electrical Events Imaged in Neurons with a Fluorescent Protein Voltage Probe. *Neuron* 75(5):779–85.
4. St-Pierre F, et al. (2014) High-fidelity optical reporting of neuronal electrical activity with an ultrafast fluorescent voltage sensor. *Nat Neurosci* 17(6):884–9.
5. Murata Y, Iwasaki H, Sasaki M, Inaba K, Okamura Y (2005) Phosphoinositide phosphatase activity coupled to an intrinsic voltage sensor. *Nature* 435(7046):1239–43.
6. Tsutsui H, et al. (2013) Improved detection of electrical activity with a voltage probe based on a voltage-sensing phosphatase. *J Physiol* 591(18):4427–37.
7. Akemann W, et al. (2012) Imaging neural circuit dynamics with a voltage-sensitive fluorescent protein. *J Neurophysiol* 108(8):2323–37.
8. Abdelfattah AS, et al. (2016) A Bright and Fast Red Fluorescent Protein Voltage Indicator That Reports Neuronal Activity in Organotypic Brain Slices. *J Neurosci* 36(8):2458–72.
9. Kralj J, Douglass A, Hochbaum D, Maclaurin D, Cohen A (2012) Optical recording of action potentials in mammalian neurons using a microbial rhodopsin.

Nat Meth 9(1):90–5.

10. Hochbaum DR, et al. (2014) All-optical electrophysiology in mammalian neurons using engineered microbial rhodopsins. *Nat Methods* 11(8):825-33.
11. Han X, et al. (2011) A High-Light Sensitivity Optical Neural Silencer: Development and Application to Optogenetic Control of Non-Human Primate Cortex. *Front Syst Neurosci* 5:18.
12. Zou P, et al. (2014) Bright and fast multicoloured voltage reporters via electrochromic FRET. *Nat Commun* 5:4625.
13. Gong Y, Wagner MJ, Zhong Li J, Schnitzer MJ (2014) Imaging neural spiking in brain tissue using FRET-opsin protein voltage sensors. *Nat Commun* 5:3674.
14. Gong Y, et al. (2015) High-speed recording of neural spikes in awake mice and flies with a fluorescent voltage sensor. *Science* 350(6266):1361–6.
15. Brinks D, Klein AJ, Cohen AE (2015) Two-Photon Lifetime Imaging of Voltage Indicating Proteins as a Probe of Absolute Membrane Voltage. *Biophysj* 109(5):914–21.
16. Cao G, et al. (2013) Genetically targeted optical electrophysiology in intact neural circuits. *Cell* 154(4):904–913.
17. Inagaki S, et al. (2017) Genetically encoded bioluminescent voltage indicator for multi-purpose use in wide range of bioimaging. *Sci Rep* 7:42398.
18. Pulver SR, Pashkovski SL, Hornstein NJ, Garrity P a, Griffith LC (2009) Temporal dynamics of neuronal activation by Channelrhodopsin-2 and TRPA1 determine behavioral output in Drosophila larvae. *J Neurophysiol*

101(6):3075–88.

19. Marshall JD, et al. (2016) Cell-Type-Specific Optical Recording of Membrane Voltage Dynamics in Freely Moving Mice. *Cell* 167(6):1650–62.e15.

20. Suzuki K, Nagai T (2017) Recent progress in expanding the chemiluminescent toolbox for bioimaging. *Curr Opin Biotechnol* 48:135–41.

21. Shaner NC, et al. (2013) A bright monomeric green fluorescent protein derived from Branchiostoma lanceolatum. *Nat Methods* 10(5):407–9.

22. Nagai T, et al. (2002) A variant of yellow fluorescent protein with fast and efficient maturation for cell-biological applications. *Nat Biotechnol* 20(1):87–90.

23. Nagai T, Yamada S, Tominaga T, Ichikawa M, Miyawaki A (2004) Expanded dynamic range of fluorescent indicators for Ca(2+) by circularly permuted yellow fluorescent proteins. *Proc Natl Acad Sci USA* 101(29):10554–9.

24. Hall MP, et al. (2012) Engineered Luciferase Reporter from a Deep Sea Shrimp Utilizing a Novel Imidazopyrazinone Substrate. *ACS Chem Biol* 7(11):1848-57

25. Sawano A, Miyawaki A (2000) Directed evolution of green fluorescent protein by a new versatile PCR strategy for site-directed and semi-random mutagenesis. *Nucleic Acids Res* 28(16):E78.

26. Tsutsui H, Jinno Y, Tomita A, Okamura Y (2013) Optically detected structural change in the N-terminal region of the voltage-sensor domain. *Biophys J* 105(1):108–15.

27. Zhao Y, et al. (2014) Microfluidic cell sorter-aided directed evolution of a protein-based calcium ion indicator with an inverted fluorescent response. *Integr*

Biol (Camb) 6(7):714–25.

28. Goldin AL (1992) Maintenance of Xenopus laevis and oocyte injection. *Methods Enzymol* 207:266–79.

29. Inutsuka A, et al. (2014) Concurrent and robust regulation of feeding behaviors and metabolism by orexin neurons. *Neuropharmacology* 85:451–60.

30. Grimm D, et al. (2008) In Vitro and In Vivo Gene Therapy Vector Evolution via Multispecies Interbreeding and Retargeting of Adeno-Associated Viruses. *J Virol* 82(12):5887–911.

31. Chamberland S, et al. (2017) Fast two-photon imaging of subcellular voltage dynamics in neuronal tissue with genetically encoded indicators. *Elife* 6: e25690.

32. Akemann W, Mutoh H, Perron A, Rossier J, Knöpfel T (2010) Imaging brain electric signals with genetically targeted voltage-sensitive fluorescent proteins. *Nat Methods* 7(8):643–9.

33. Takahashi K, Yamanaka S (2006) Induction of Pluripotent Stem Cells from Mouse Embryonic and Adult Fibroblast Cultures by Defined Factors. *Cell* 126(4):663–76.

34. Thomson JA, et al. (1998) Embryonic Stem Cell Lines Derived from Human Blastocysts. *Science* 282(5391):1145–7.

35. Shinnawi R, et al. (2015) Monitoring Human-Induced Pluripotent Stem Cell-Derived Cardiomyocytes with Genetically Encoded Calcium and Voltage Fluorescent Reporters. *Stem Cell Reports* 5(4):582–96.

36. Chang Y, et al. (2017) Non-invasive phenotyping and drug testing in single

cardiomyocytes or beta-cells by calcium imaging and optogenetics. *PLoS One* 12(4):e0174181.

37. Leyton-Mange JS, et al. (2014) Rapid cellular phenotyping of human pluripotent stem cell-derived cardiomyocytes using a genetically encoded fluorescent voltage sensor. *Stem Cell Reports* 2(2):163–70.

38. Doss MX, et al. (2012) Maximum diastolic potential of human induced pluripotent stem cell-derived cardiomyocytes depends critically on IKr. *PLoS One* 7(7): e40288.

39. Mandel Y, et al. (2012) Human embryonic and induced pluripotent stem cell-derived cardiomyocytes exhibit beat rate variability and power-law behavior. *Circulation* 125:883–93.

40. Scheel O, et al. (2014) Action Potential Characterization of Human induced pluripotent stem cell-derived cardiomyocytes using automated patch-clamp technology. Assay Drug Dev Technol. 12(8):457–69.

41. Gibson JK, Yue Y, Bronson J, Palmer C, Numann R (2014) Journal of Pharmacological and Toxicological Methods Human stem cell-derived cardiomyocytes detect drug-mediated changes in action potentials and ion currents. *J Pharmacol Toxicol Methods* 70(3):255–67.

42. Gradinaru V, et al. (2010) Molecular and Cellular Approaches for Diversifying and Extending Optogenetics. *Cell* 141(1):154–65.

43. Lin JY (2011) A user's guide to channelrhodopsin variants: features, limitations and future developments. *Exp Physiol* 96(1):19–25.

44. Kim JH, et al. (2011) High cleavage efficiency of a 2A peptide derived from porcine teschovirus-1 in human cell lines, zebrafish and mice. *PLoS One* 6(4):e18556.

45. Chang YF, Arai Y, Nagai T (2012) Optogenetic activation during detector " dead time" enables compatible real-time fluorescence imaging. *Neurosci Res* 73(4):341–7.

46. Saito K, et al. (2012) Luminescent proteins for high-speed single-cell and whole-body imaging. *Nat Commun* 3:1262.

47. Bridges CD (1971) The molar absorbance coefficient of rhodopsin. *Vision Res* 11(8):841-8.

48. Lakowicz, JR. (2006) Principles of Fluorescence Spectroscopy Springer Science, New York.

49. Deisseroth K (2015) Optogenetics: 10 years of microbial opsins in neuroscience. *Nat Neurosci* 18(9):1213–25.

50. Buzsáki G, Anastassiou CA, Koch C (2012) The origin of extracellular fields and currents--EEG, ECoG, LFP and spikes. *Nat Rev Neurosci* 13(6):407–20.

51. Mohajerani MH, et al. (2013) Spontaneous cortical activity alternates between motifs defined by regional axonal projections. *Nat Neurosci* 16(10):1426–35.

52. Madisen L, et al. (2015) Transgenic Mice for Intersectional Targeting of Neural Sensors and Effectors with High Specificity and Performance. *Neuron* 85(5):942-58..

53. Agetsuma M, Hamm JP, Tao K, Fujisawa S, Yuste R (2017)

Parvalbumin-Positive Interneurons Regulate Neuronal Ensembles in Visual Cortex. *Cereb Cortex* In press.

54. Herry C, et al. (2008) Switching on and off fear by distinct neuronal circuits. *Nature* 454(7204):600–6.

55. Chen TW, et al. (2013) Ultrasensitive fluorescent proteins for imaging neuronal activity. *Nature* 499(7458):295–300.

56. Keller GB, Bonhoeffer T, Hübener M (2012) Sensorimotor mismatch signals in primary visual cortex of the behaving mouse. *Neuron* 74(5):809–15.

57. Saleem AB, Ayaz A, Jeffery KJ, Harris KD, Carandini M (2013) Integration of visual motion and locomotion in mouse visual cortex. *Nat Neurosci* 16(12):1864–1869.

58. Fu Y, et al. (2014) A Cortical Circuit for Gain Control by Behavioral State. *Cell* 156(6):1139–1152.

59. Higashi A, Uchizono K, Tani Y, Hoshino M, Yano T YK (1979) Real time online data processing system for the e.e.g, and body movement during the lifetime of a freely moving mouse. *Med Biol Eng Comput* 17(3):416–8.

60. Ferezou I, Bolea S, Petersen CCH (2006) Visualizing the Cortical Representation of Whisker Touch: Voltage-Sensitive Dye Imaging in Freely Moving Mice. *Neuron* 50(4):617–629.

61. Ziv Y, Ghosh KK (2015) Miniature microscopes for large-scale imaging of neuronal activity in freely behaving rodents. *Curr Opin Neurobiol* 32:141–47.

62. Miyamoto D, Murayama M (2016) The fiber-optic imaging and manipulation of

neural activity during animal behavior. *Neurosci Res* 103:1–9.

63. Matsushita J, et al. (2017) Fluorescence and Bioluminescence Imaging of Angiogenesis in Flk1-Nano-lantern Transgenic Mice. *Sci Rep* 7:46597.

64. Wang Y, et al. (2014) Single molecule FRET reveals pore size and opening mechanism of a mechano-sensitive ion channel. *Elife* 3:e01834.

65. de Chaumont F, et al. (2012) Computerized video analysis of social interactions in mice. *Nat Methods* 9(4):410–417.

66. Montgomery KL, et al. (2015) Wirelessly powered, fully internal optogenetics for brain, spinal and peripheral circuits in mice. *Nat Methods* 12(10):969–974.

67. Inagaki, S., Agetsuma, M., Ohara, S., Iijima,T., Wazawa,T., Arai,Y., Nagai,T. *In vivo* brain activity imaging of interactively locomoting mice. Submitted.

Achievement

Original papers

1. **Inagaki, S*(equal contribution)**., Agetsuma, M*., Ohara, S., Iijima, T., Wazawa, T., Arai, Y., Nagai, T. *In vivo* brain activity imaging of interactively locomoting mice. **Submitted.** (The author established the fiber-free imaging system, conducted *in vitro* characterization with Dr. Ohara and performed *in vivo* experiments with Dr. Agetsuma.)
2. Matsushita, J*., **Inagaki, S*(equal contribution)**., Nishie, T., Sakasai, T., Tanaka, J., Watanabe, C., Mizutani, K., Miwa, T., Matsumoto, K., Takara, K., Naito, H., Kidoya, H., Takakura, N., Nagai, T., Takahashi, S., Ema, M. Fluorescence and Bioluminescence Imaging of Angiogenesis in Flk1-Nano-lantern Transgenic Mice. ***Scientific Reports***. 7, 46597, 2017 (The author performed *ex* and *in vivo* chemiluminescence imaging.)
3. **Inagaki, S.**, Tsutsui, H., Suzuki, K., Agetsuma, M., Arai, Y., Jinno, Y., Bai, G., Daniels, M.J, Okamura, Y., Matsuda, T., Nagai, T. Genetically encoded bioluminescent voltage indicator for multi-purpose use in wide range of bioimaging. ***Scientific Report*s.** 7, 42398, 2017. (The author developed a chemiluminescent voltage indicator and performed experiments except for electrophysiology.)

Reviews

1. 鈴木和志・**稲垣成矩**・永井健治/ 化学発光と蛍光（ナノ・ランタン）/**再生**

医療, In preparation.

2. **Inagaki, S**., Nagai, T. Current progress in genetically encoded voltage indicators for neural activity recording. ***Current Opinion In Chemical Biology*,** 33, 95-100, 2016.
3. **稲垣成矩**・永井健治/ 遺伝子にコードされた膜電位センサーによる神経活動計測の現状と展望/ ***Drug Delivery System*,** 31-2, 119-126, 2016.

Proceedings

1. **Inagaki S*(equal contribution).,** Agetsuma, M*., Nagai T. A novel fiber-free technique for brain activity imaging in multiple freely behaving mice. ***Proc. SPIE.*** 10482, 2018 (The author established the fiber-free imaging system and performed *in vivo* experiments with Dr. Agetsuma.)
2. **Inagaki S.,** Nagai T. Bioluminescent indicator applicable to voltage recording in various excitable cell types. ***Proc. SPIE.*** 1025102, 2017.
3. Thammasan, N., Iwano, M., Moriyama, K., Fukui, K., Kawintiranon, K., Buatong, Y., **Inagaki, S.**, Nagai, T., and Numao, M. An Investigation of Effect of Bioluminescent Light on Human using Electroencephalogram. ***Proc. The 23nd International Display Workshop in conjunction with Asia Display*,** pp. 57-60, Fukuoka, Japan, Dec. 2016. (The author helped to set up the lightning system and become a subject for EEG recording)

Preprints

1. **Inagaki, S.*,** Agetsuma, M.*(equal contribution), Ohara, S., Iijima, T., Wazawa, T., Arai, Y., Nagai, T. *In vivo* brain activity imaging of interactively locomoting mice. ***bioRxiv.*** DOI: https://doi.org/10.1101/203422. (The author established the fiber-free imaging system, conducted *in vitro* characterization with Dr. Ohara and performed *in vivo* experiments with Dr. Agetsuma.)

Books

1. 鈴木和志・**稲垣成矩**・永井健治/ 蛍光・化学発光ライブイメージングの現状と展望/ **第43回組織細胞化学講習会テキスト/ Submitted**.

Awards

1. **Poster Award for Young Scientist**　The 20th ISIR International Symposium
2. **優秀ポスター賞**　第39回日本分子生物学会年会
3. **学生発表賞**　第54回日本生物物理学会年会
4. **Janelia Conference Scholarship** (Fluorescent Proteins and Biological sensors IV. (2014))

Oral presentation (international)

1. **Inagaki, S.**, Matsuda, T., Arai, Y., Jinno, Y., Tsutsui, H., Okamura, Y., Nagai, T. Genetically-encoded chemiluminescent voltage indicator applicable in millisecond voltage phenomena. CaBP19, Vanderbilt Univ, USA, 30 May.-3 June. 2015.
2. **Inagaki, S.**, Matsuda, T., Arai, Y., Jinno, Y., Tsutsui, H., Okamura, Y., Nagai, T.

Genetically-encoded chemiluminescent voltage indicator applicable in conjunction with multiple optogenetic tools. Next Generation Sensor Devices for a Healthier, Safer Society International Networking Workshop. University of Oxford, UK, 24-25 Jul. 2014. **[Invited speech]**

Poster presentation (international)

1. **Inagaki, S.,** Agetsuma, M., Ohara, S., Iijima, T., Wazawa, T., Arai, Y., Nagai, T. Genetically encoded chemiluminescent voltage indicator applicable to brain activity recording in freely moving mice. 9th Optogenetics Research Society Japan International Symposium, Tohoku University, Japan, 21 Oct. 2017
2. **Inagaki, S.,** Agetsuma, M., Hidekazu, T., Ohara, S., Arai, Y., Suzuki, K., Jinno, Y., Matsuda, T., Iijima, T., Okamura, Y. Nagai, T. Chemiluminescent voltage indicator applicable to brain activity recording in freely moving mice. Humanware International Symposium 2017, Senri Hankyu Hotel, Japan, 26 Jan. 2017.
3. **Inagaki, S.,** Agetsuma, M., Hidekazu, T., Ohara, S., Arai, Y., Suzuki, K., Jinno, Y., Matsuda, T., Iijima, T., Okamura, Y. Nagai, T. Chemiluminescent voltage indicator applicable to brain activity recording in freely moving mice. The 20th ISIR International Symposium, Knowledge Capital Congrès Convention Center, Japan, 12 - 13 Dec. 2016.
4. **Inagaki, S.**, Agetsuma, M., Tsutsui, H., Matsuda., Arai, Y., Jinno, Y., Bai, G., Suzuki, K., Daniels, M.J., Okamura, Y. and Nagai, T. Genetically-encoded chemiluminescent indicator applicable in milli-second voltage phenomena. The

International Chemical Congress of Pacific Basin Societies, Honolulu, Hawaii, USA, 15-20 Dec. 2015.

5. **Inagaki, S.,** Matsuda, T., Arai, Y., Jinno, Y., Tsutsui, H., Okamura, Y. and Nagai, T. Genetically-encoded chemiluminescent voltage indicator applicable in conjunction with multiple optogenetic tools. Fluorescent Proteins and Biological sensors IV. Janelia Research Campus, USA, 28 Sep.-1 Oct. 2014.

Oral presentation (domestic)

1. 稲垣成矩・揚妻正和・筒井秀和・大原慎也・新井由之・神野有香・白貴蓉・飯島敏夫・Matthew J. Daniels・岡村康司・松田知己・永井健治 /複数の自由行動マウスにおける脳活動計測が可能な化学発光膜電位センサーの開発 / 第55回日本生物物理学会年会 /熊本大学 2017年9月19日-21日
2. 稲垣成矩・揚妻正和・筒井秀和・大原慎也・新井由之・鈴木和志・神野有香・松田知己・飯島敏夫・岡村康司・永井健治 / 複数マウスの脳活動を自由行動下で同時計測可能な化学発光膜電位センサーの開発 / 第40回日本神経科学大会 /幕張メッセ 2017年7月20日-23日
3. 稲垣成矩 / 自由行動マウスの脳活動計測を可能にする化学発光膜電位センサーの開発 / 蛋白研セミナー「膜タンパク質の構造ダイナミクス」/ 大阪大学蛋白質研究所 2016年5月12日-13日 **[招待講演]**
4. 稲垣成矩・揚妻正和・松田知己・新井由之・白貴蓉・神野有香・筒井秀和・Matthew J. Daniels・岡村康司・永井健治 / 複数の光遺伝学操作と組み合わせたイメージングと薬剤スクリーニングの可能性を広げる発光膜電位指示

薬の開発 / 第38回日本分子生物学会年会/ 神戸ポートアイランド 2015年12月1日- 4日

5. 稲垣成矩・松田知己・揚妻正和・新井由之・白貴蓉・神野有香・筒井秀和・岡村康史・永井健治 / 複数の光遺伝学操作と組み合わせたイメージングと薬剤スクリーニングの可能性を広げる発光膜電位指示薬の開発 /第53回日本生物物理学会年会/ 金沢大学 2015年9月13日-15日
6. 稲垣成矩・松田知己・揚妻正和・新井由之・白貴蓉・神野有香・筒井秀和・岡村康司・永井健治 / 複数の光遺伝学操作と組み合わせたイメージングと薬剤スクリーニングの可能性を広げる化学発光膜電位指示薬の開発 / 平成27年度生理学研究所研究会「生体シグナルダイナミクス」2015年9月3日 - 4日[**招待講演**]

Poster presentation (domestic)

1. 稲垣成矩・揚妻正和・筒井秀和・新井由之・鈴木和志・神野有香・岡村康司・松田知己・永井健治 / 自由行動マウスの脳活動計測を可能にする化学発光膜電位センサーの開発 / 第39回日本分子生物学会年会/ パシフィコ横浜 2016年11月30日- 12月1日
2. 稲垣成矩・揚妻正和・筒井秀和・新井由之・鈴木和志・神野有香・岡村康司・松田知己・永井健治 / 自由行動マウスの脳活動計測を可能にする化学発光膜電位センサーの開発 / 第54回日本生物物理学会年会/ つくば国際会議場 2016年11月25日- 27日
3. **Inagaki, S.,** Agetsuma, M., Tsutsui, H., Arai, Y., Suzuki, K., Jinno, Y., Okamura,

Y., Matsuda, T. and Nagai, T. Development of a chemiluminescent voltage indicator applicable to brain activity recording in freely moving mice/ QBiC Symposium 2016 Decoding Organisms by Quantitative Cell Profiling/Senri Life Science Center, Japan, 5 - 7 Sep. 2016.

4. 稲垣成矩・松田知己・新井由之・白貴蓉・神野有香・筒井秀和・岡村康司・永井健治/ 複数の光操作と組み合わせた膜電位メージングと薬剤スクリーニングの可能性を広げる発光指示薬の開発/ 2015アライアンスG3分科会/ 大阪大学会館 2015年11月12日

5. 稲垣成矩・松田知己・新井由之・神野有香・筒井秀和・岡村康司・永井健治/ 複数の光遺伝学ツールと組み合わせ可能な、化学発光膜電位センサーの開発/ 第37回日本分子生物学会年会/ パシフィコ横浜 2014年11月25日-27日

6. 稲垣成矩・松田知己・新井由之・神野有香・筒井秀和・岡村康司・永井健治 / Genetically-encoded chemiluminescent voltage indicator applicable in conjunction with multiple optogenetic tools/ 第52回日本生物物理学会年会/ 札幌コンベンションセンター 2014年9月25日-27日

7. 稲垣成矩・松田知己・新井由之・神野有香・筒井秀和・岡村康司・永井健治/ 遺伝子にコードされた化学発光膜電位センサーの開発/ 附置研究所間アライアンスによるナノとマクロをつなぐ物質・デバイス・システム創製プロジェクト・平成25年度成果報告会/ 大阪大学　2014年5月30日

This thesis was written based on the content of following papers;

- Inagaki, S., Agetsuma, M., Ohara, S., Iijima, T., Wazawa, T., Arai, Y., Nagai, T. *In vivo* brain activity imaging of interactively locomoting mice. **Submitted.**
- Inagaki, S., Tsutsui, H., Suzuki, K., Agetsuma, M., Arai, Y., Jinno, Y., Bai, G., Daniels, M.J, Okamura, Y., Matsuda, T., Nagai, T. Genetically encoded bioluminescent voltage indicator for multi-purpose use in wide range of bioimaging. ***Scientific Report*s.** 7, 42398, 2017.